Multiwavelength Ranging/Streak Cameras

N94-15580

OPTIMUM WAVELENGTHS FOR TWO COLOR RANGING

John J. Degnan
Code 901/ Crustal Dynamics Project
NASA Goddard Space Flight Center
Greenbelt, MD 20771

ABSTRACT

The range uncertainties associated with the refractive atmosphere can be mitigated by the technique of two color, or dual wavelength, ranging. The precision of the differential time of flight (DTOF) measurement depends on the atmospheric dispersion between the two wavelengths, the received pulsewidths and photoelectron counts, and on the amount of temporal averaging. In general, the transmitted wavelengths are not independently chosen but instead are generated via nonlinear optics techniques (harmonic crystals, Raman scattering, etc.) which also determine their relative pulsewidths. The mean received photoelectrons at each wavelength are calculated via the familiar radar link equation which contains several wavelength dependent parameters. By collecting the various wavelength dependent terms, one can define a wavelength figure of merit for a two color laser ranging system.

In this paper, we apply the wavelength figure of merit to the case of an extremely clear atmosphere and draw several conclusions regarding the relative merits of fundamental-second harmonic, fundamental-third harmonic, second-third harmonic, and Raman two color systems. We find that, in spite of the larger dispersion between wavelengths, fundamental-third harmonic systems have the lowest figure of merit due to a combination of poor detector performance at the fundamental and poor atmospheric transmission at the third harmonic. Fundamental-second harmonic (~700 nm and 350 nm) have the highest figure of merit, but second-third harmonic systems, using fundamental transmitters near 1000 nm, are a close second. Raman-shifted transmitters appear to offer no advantage over harmonic systems because of (1) the relatively small wavelength separation that can be achieved in light gases such as hydrogen and (2) the lack of good ultrashort pulse transmitters with an optimum fundamental wavelength near 400 nm.

1 INTRODUCTION

With the subcentimeter precisions available from modern satellite laser ranging (SLR) hardware [Degnan, 1985], atmospheric refraction is a dominant error source in the absolute determination of the geometric range from the station to the satellite. While atmospheric modelling is believed to reduce the systematic errors to roughly one centimeter or less, future progress toward millimeter absolute accuracy ranging will rely on the technique of two color, or dual wavelength, ranging.

In the present paper, we attempt to define optimum wavelengths for two color ranging. In order to accomplish this, we must take into account all of the wavelength dependent parameters which influence our ability to make an accurate differential time of flight (DTOF) measurement. As we will see in the ensuing sections, a proper accounting of wavelength dependent terms will include atmospheric dispersion, atmospheric transmission as a function of sea level visibility, transmit antenna and target gains, detector responsivities, transmitter availability and pulsewidth, and the detailed characteristics of the available nonlinear optics techniques for achieving the necessary optical frequency translations.

2 ATMOSPHERIC REFRACTION: THE MARINI-MURRAY MODEL

In the Marini-Murray model of atmospheric refraction [Marini and Murray, 1973], radial variability in the meteorological parameters (i.e. with altitude) is assumed to be governed by the equations for hydrostatic equilibrium, the law of partial pressures, and the perfect gas law. This leads to the following equations for the spherical range correction, SC_{MM}:

$$SC_{MM}(\lambda,E,P_H,T_H,e_H)=\frac{f(\lambda)}{F(\phi,H)}\frac{A(P_H,e_H)+B(\phi,T_H,P_H)}{\sin(E)+\frac{B(\phi,T_H,P_H)}{\frac{A(P_H,e_H)+B(\phi,T_H,P_H)}{\sin E+.01}}} \tag{2.1}$$

where

$$f(\lambda)=.9650+\frac{.0164}{\lambda^2}+\frac{.000228}{\lambda^4} \tag{2.2a}$$

$$F(\phi,H)=1-.0026\cos 2\phi-.00031H \tag{2.2b}$$

$$A(P_H,e_H)=.002357P_H+.000141e_H \tag{2.2c}$$

$$B(\phi,T_H,P_H)=1.084x10^{-8}P_HT_HK(\phi,T_H,P_H)+4.734x10^{-8}\frac{P_H^2}{T_H}\frac{2}{3-\frac{1}{K(\phi,T_H,P_H)}} \tag{2.2d}$$

and

$$K(\phi,T_H,P_H)=1.163-.00968\cos 2\phi-.00104T_H+.0001435P_H \tag{2.2e}$$

where λ is the laser wavelength in microns, E is the true elevation angle of the satellite in degrees, ϕ is the station latitude, H is the station height above mean sea level, and P_H, T_H and e_H are the surface pressure, temperature, and water vapor pressure at the station. The water vapor pressure e_H is related to the surface percent relative humidity R_H and surface temperature T_H by the equation

$$e_H(R_H, T_H) = \frac{R_H}{100} 6.11 x 10^{\left(7.5 \frac{T_H - 273.15}{237.3 + (T_H - 273.15)}\right)} \tag{2.3}$$

The wavelength dependence of the range correction is contained in the dispersion term $f(\lambda)$ which is plotted in Figure 1. It was arbitrarily chosen by Marini and Murray to have a value of unity at the ruby laser wavelength of .6943 microns.

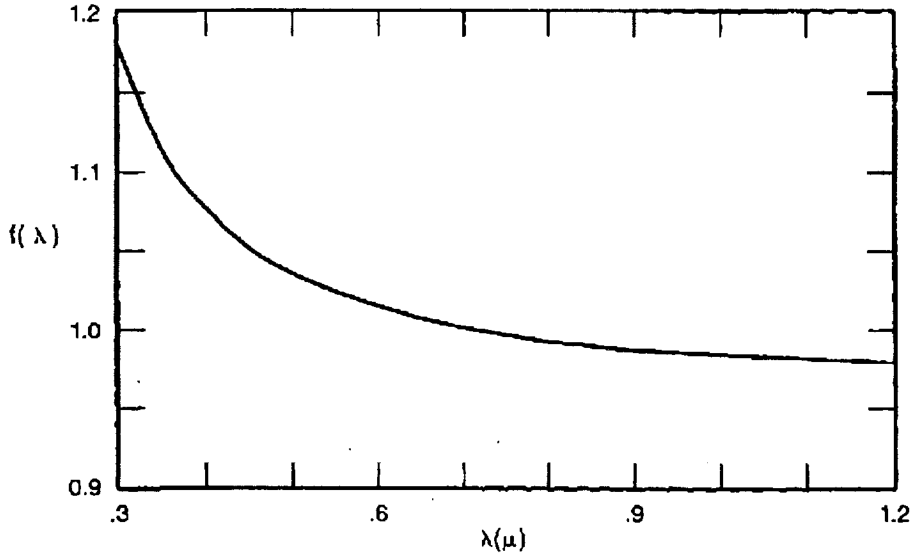

Figure 1. Atmospheric dispersion in a standard atmosphere as a function of wavelength from the near ultraviolet to the near infrared.

3 TWO-COLOR LASER RANGING

By measuring the pulse times-of-flight at two colors and multiplying the results by the velocity of light in vacuum, c, we obtain a measure of the optical path lengths through the atmosphere at the two wavelengths. Thus, the atmospheric refraction correction is given by

$$AC = \gamma(L_1 - L_2) = \frac{\gamma c}{2}(\tau_1 - \tau_2) \tag{3.1}$$

where L_1 and L_2 are the optical path lengths and τ_1 and τ_2 are the measured roundtrip times of flight at the two wavelengths respectively, and

$$\gamma = \frac{n_{g1} - 1}{n_{g2} - n_{g1}} \tag{3.2}$$

where n_{g1} and n_{g2} are the group refractive indices at the two wavelengths. Unfortunately, the wavelength dependence due to the "dry" and "wet" components of the atmosphere are different [Owens, 1968] whereas the expression for the group refractivity N_g used by Marini and Murray assumes no dependence of the water vapor term on wavelength, i.e.

$$N_g(\lambda) = 80.343 f(\lambda)\frac{P}{T} - 11.3\frac{e}{T} \tag{3.3}$$

where P, T, and e are the local pressure, temperature, and water vapor partial pressure respectively. Nevertheless, under normal conditions of modest humidity, γ can be well approximated by the expression [Abshire and Gardner, 1985]

$$\gamma = \frac{f(\lambda_1)}{f(\lambda_2) - f(\lambda_1)} \tag{3.4}$$

where $f(\lambda)$ is given by (2.2a). If we assume that the two times of flight are independently measured, we can express the expected variance in the atmospheric correction as

$$\sigma_{AC}^2 = (\gamma c/2)^2(\sigma_1^2 + \sigma_2^2) \tag{3.5}$$

where σ_1 and σ_2 are the RMS errors in the time of flight measurements at the wavelengths λ_1 and λ_2 respectively. In the ideal limit where the differential timing precision is determined only by the signal strength, one can write

$$\sigma_{AC} = \frac{\gamma c}{2}\left(\frac{\tau_{p1}^2}{n_1} + \frac{\tau_{p2}^2}{n_2}\right)^{1/2} \tag{3.6}$$

where τ_{p1} and τ_{p2} are the laser pulsewidths and n_1 and n_2 are the received photoelectron signal strengths at the two wavelengths respectively.

4 THE RADAR LINK EQUATION

The mean signal flux in a range receiver is obtained from the familiar radar link equation. The mean number of photoelectrons n_{pe} recorded by the ranging detector is given by:

$$n_{pe} = \eta_q \left(E_T \frac{\lambda}{hc} \right) \eta_t G_t \sigma \left(\frac{1}{4\pi R^2} \right)^2 A_r \eta_r T_a^2 T_c^2 \qquad (4.1)$$

where η_q is the detector quantum efficiency, E_T is the laser pulse energy, λ is the laser wavelength, h is Planck's constant, c is the velocity of light in vacuum, η_t is the transmit optics efficiency, G_t is the transmitter gain, σ is the satellite optical cross-section, R is the slant range to the target, A_r is the effective area of the telescope receive aperture, η_r is the efficiency of the receive optics, T_a is the one-way atmospheric transmission, T_c is the one way transmissivity of cirrus clouds (when present), and R is the slant range between the station and the target.

In discussing the link equation, we are primarily concerned with those terms which exhibit a wavelength dependence. While optical coatings certainly exhibit a wavelength dependence thereby affecting the transmit and receive optical efficiencies η_t and η_r, coatings can generally be designed to give approximately equal performance once the operating wavelengths are chosen and hence will not be included in our discussion. Similarly, experimental studies of cirrus cloud transmission have shown no significant dependence on wavelength over the band from 0.317 to 12 microns. Other terms in (4.1) do have a wavelength dependence which we will now discuss.

4.1 TRANSMITTER GAIN

A general expression for the transmitter gain is given by

$$G_t = \frac{4\pi A_t}{\lambda^2} g_t(\alpha_t, \beta, \gamma_t, X) \qquad (4.2)$$

where $A_t = \pi a^2$ is the area of the transmitting aperture and $g_t(\alpha_t, \beta, \gamma_t, X)$ is a geometric factor independent of wavelength [Klein and Degnan, 1974]. Note that, for a given transmit aperture and a well-collimated system, the transmitter gain is inversely proportional to the wavelength squared.

4.2 TARGET OPTICAL CROSS-SECTION

The optical cross-section of an unspoiled retroreflector is given by [Degnan, 1992]

$$\sigma_{cc} = \rho A_{cc} \left(\frac{4\pi A_{cc}}{\lambda^2} \right) \qquad (4.3)$$

where ρ is the cube corner reflectivity, $A_{cc} = \pi R_{cc}^2$ is the light collecting area of the corner cube, and $4\pi A_{cc}/\lambda^2$ is the on-axis retroreflector gain. Even in the presence of complicating factors such as velocity aberration and retroreflector spoiling, an array of retroreflectors designed to operate at both wavelengths would be expected to retain the same inverse square law dependence on wavelength exhibited by (4.3).

4.3 ATMOSPHERIC ATTENUATION

In the near-ultraviolet to visible spectral band between 0.3 and 0.7 μ, atmospheric attenuation is dominated by aerosol (Mie) scattering but molecular (Rayleigh) and ozone absorption also play a role [RCA, 1968]. In the near infrared beyond 0.7μ, the plot of atmospheric transmission versus wavelength (see Figure 2) is modulated by strong absorption features of various molecular constituents in the atmosphere, notably water vapor, oxygen, and carbon dioxide.

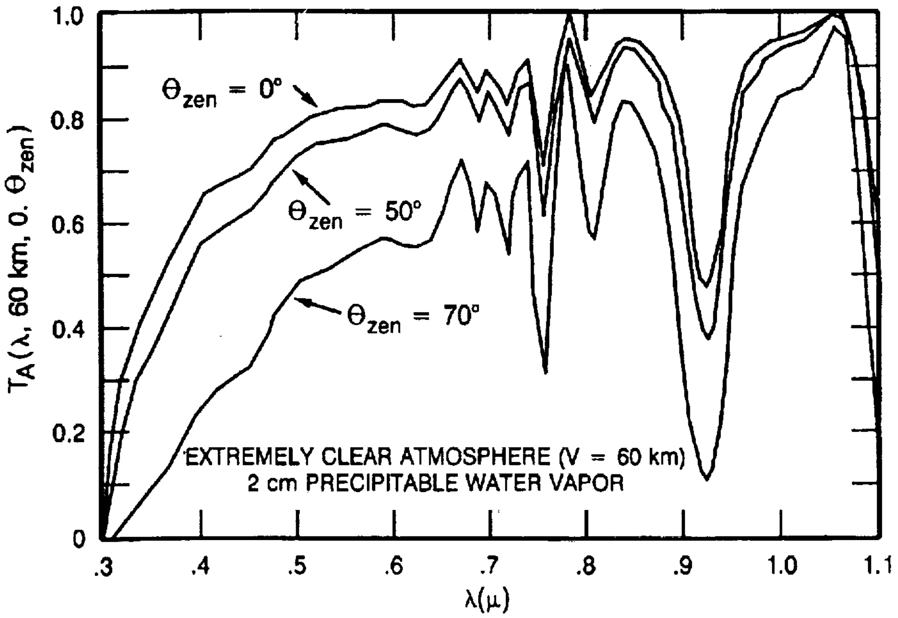

Figure 2. Atmospheric transmission as a function of wavelength under extremely clear conditions with 2 cm of precipitable water vapor at zenith angles of 0, 50, and 70^{o} (corresponding to 1, 2, and 3 air masses) respectively.

The transmission curve presented in Figure 2 corresponds to excellent "seeing" conditions (80 Km visibility) and 2 cm of precipitable water vapor. It should be noted that atmospheric seeing conditions vary widely from day to day and from site to site and are usually characterized by "sea level visibility" expressed in kilometers. Plots of the sea level attenuation coefficient versus wavelength (from 0.4 to 4 μ) as a function of sea level visibility can be found in the RCA Electro-Optics

Handbook [RCA,1968]. For the purpose of this analysis, however, we will consider only the extremely clear atmosphere depicted in Figure 2.

4.4 OPTICAL DETECTORS

Finally, the availability of high quantum efficiency optical detectors at the two laser wavelengths is important. If a common photocathode is to be used, such as in most streak camera schemes for performing differential timing, the photocathode must be sensitive at both wavelengths. However, since the images of the two return pulses can be spatially separated in the entrance slit of the streak camera, one can conceive of specially constructed streak tubes containing more than one photocathode material to obtain the highest sensitivity at both wavelengths. It may also be possible, at some future date, to do the necessary timing via electronic means, such as high speed GaAs technology, without resorting to streak camera technology although this capability has not yet been demonstrated.

A) "BEST" PHOTOEMISSIVE DETECTOR RESPONSIVITIES

WAVELENGTH (μ)	RESPONSIVITY	PHOTOCATHODE (+ WINDOW) MATERIAL
.3	50	S20
.35	60	K-Cs-Sb + (LIME GLASS)
.40	80	K-Cs-Sb + (LIME GLASS)
.45	70	K-Cs-Sb + (LIME GLASS)
.50	63	K-Cs-Sb + (LIME GLASS)
.55	64	GaAs (+ 9741 GLASS)
.60	65	GaAs (+ 9741 GLASS)
.65	67	GaAs (+ 9741 GLASS)
.70	68	GaAs (+ 9741 GLASS)
.75	69	GaAs (+ 9741 GLASS)
.80	70	GaAs (+ 9741 GLASS)
.85	58	GaAs (+ 9741 GLASS)
.90	13	GaAs (+ 9741 GLASS)
.98	9	GaInAs (+ 9741 GLASS)
1.02	.8	GaInAs (+ 9741 GLASS)
1.1	.2	S1

B) COMPOSITE GRAPH OF PHOTOEMISSIVE DETECTOR RESPONSIVITY

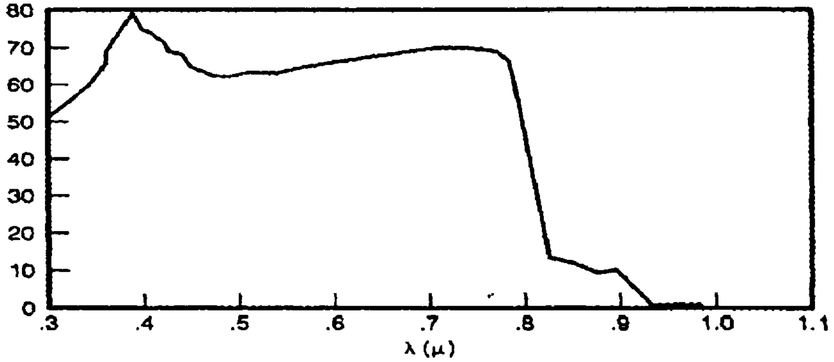

Figure 3. Summary of "best" photoemissive detector responsivities from the near ultraviolet to the near infrared.

Detector sensitivity at a particular wavelength is usually expressed as "spectral responsivity" in milliamperes/Watt. It is related to quantum efficiency by the equation

$$\eta_q(\lambda) = R(\lambda)\frac{hc}{\lambda e} \tag{4.4}$$

where $R(\lambda)$ is the detector spectral responsivity at wavelength λ, h is Planck's constant, and c is the velocity of light. A composite responsivity curve, which is the envelope of individual responsivity curves for some common visible and near infrared photoemissive detectors[Slater, 1980; Zwicker, 1977] is illustrated in Figure 3.

5 "OPTIMUM" WAVELENGTHS FOR TWO COLOR SLR

In choosing "optimum" candidate wavelengths for successful two color ranging, there are a variety of technical issues the engineer must consider. These will be discussed in the ensuing subsections. As we shall now see, equation (3.6) for the RMS error in the atmospheric correction for the photon-limited case, combined with the radar link equation (4.1), points the way to the selection of a set of optimum wavelengths. Since we want to minimize σ_{AC}, the inverse of (3.6) can serve as an overall system figure of merit.

5.1 ATMOSPHERE

The dependence of (3.6) on the atmospheric dispersive function $f(\lambda)$ illustrates the need for adequate atmospheric dispersion between the two wavelengths in order to reduce the severity of the timing requirements. The atmospheric dispersion curve in Figure 1 strongly suggests that one wavelength be chosen to lie in the near ultraviolet. On the other hand, atmospheric attenuation in the spectral band between 0.3 and 0.7 microns, resulting from the combined effects of molecular (Rayleigh) and aerosol (Mie) scattering and ozone absorption, also increases rapidly in the near ultraviolet as shown in Figure 2. This will negatively impact the timing precision by lowering the photoelectron count at the UV wavelength. Furthermore, in choosing a laser wavelength, it is probably wise to avoid the strong water absorption lines in the spectral regions between 0.7 and 1.0 microns and beyond 1.1 micron. The high variability of water vapor total burden would impact both the day-to-day signal strength and cause the pulse group velocity to vary via the anomalous dispersion effect near an absorbing feature.

5.2 LASER TRANSMITTER

The availability of lasers capable of generating high peak powers and ultrashort pulsewidths on the order of 35 picoseconds or less is also a consideration. Preference is generally given to solid state lasers because of the practical difficulties of using liquid dye lasers in the field. Over the past decade, much progress has been made in the development of highly tunable solid state lasers such as Alexandrite (700 to 810 nm) and Titanium-doped sapphire (600 to 900 nm). The wide bandwidths of these new materials are capable of supporting subpicosecond pulsewidths whereas today's workhorse, Nd:YAG, is limited to about 10 picoseconds by it's relatively narrow linewidth (120 GHz). However, high bandwidth comes at a price - i.e. lower gain - making the construction of high peak power Ti:Sapphire and Alexandrite devices more difficult.

Generally, the wavelengths in two color systems are generated from the fundamental wavelength λ_f via nonlinear optical techniques such as harmonic generation in crystals or Raman shifting in gases. This assures simultaneity of emission and eliminates (thankfully) the need to synchronize the firings of two separate lasers with picosecond precisions. However, reliance on nonlinear teqhniques implies that the two wavelengths cannot be chosen independently of each other. In the case of harmonic generation, the second and third harmonic wavelengths are given by

$$\lambda_2 = \frac{\lambda_1}{2} \qquad \lambda_3 = \frac{\lambda_1}{3} \tag{5.1}$$

respectively.

In Raman shifting, a portion of the incident radiation at input frequency, ν_o is shifted by some fixed amount ν_s (the "Stokes shift") toward longer wavelengths relative to the fundamental. One also obtains frequencies at longer ("Stokes") and shorter ("Anti-Stokes") wavelengths, but these are generally too weak to supply sufficient energy for satellite ranging. Large Stokes frequency shifts, and hence high dispersion between wavelengths, are obtained by Raman shifting in light gases. Hydrogen produces the largest shift of 4155 cm^{-1}, and photon conversion efficiencies as high as 80% have been reported. For example, one proposed two color SLR system uses the second harmonic of Nd:YAG (532 nm) in hydrogen to obtain a second wavelength output at 680 nm [Gaignebet et al, 1986].

A second consequence of harmonic or Raman generation is that the pulsewidth of the secondary wavelength is generally shorter than the pulsewidth of the fundamental. From the theory of harmonic generation [Degnan, 1979], the harmonic pulsewidths are approximately given by

$$\tau_{2h} \sim \frac{\tau_1}{\sqrt{2}} \qquad \tau_{3h} \sim \frac{\tau_1}{\sqrt{3}} \tag{5.2}$$

for low to moderate energy conversion efficiencies (< 50% - the usual case). Raman generation depends on third order nonlinear processes, and the pulsewidth dependence is identical to that of third harmonic generation.

5.3 WAVELENGTH FIGURE OF MERIT

In order to treat all potential system configurations on an equal basis, some assumptions are in order. We will assume that the fundamental laser, from which all other wavelengths are derived, is characterized by an energy E and a pulsewidth τ_p which is constant for all wavelengths. Thus, Equation (3.6) becomes

$$\sigma_{AC} = \gamma c \tau_p \sqrt{\frac{1}{\beta_1^2 n_1} + \frac{1}{\beta_2^2 n_2}} \tag{5.3}$$

where β_1 and β_2 are pulsewidth scale factors which depend on the nonlinear process used to generate them as in (5.2). In addition, we recognize that wavelengths derived via nonlinear processes are obtained with some typical energy efficiency which we will denote by η_1 and η_2 respectively. If the fundamental wavelength is used as one of the two wavelengths, we will assign values of $\beta_f = 1$ and $\eta_f = 1$. For second and third harmonic generation in the ultrashort pulse regime, typical conversion efficiencies are $\eta_{sh} = .5$ and $\eta_{th} = .2$ respectively.

In order to derive a wavelength figure of merit, we must now bring together all of the wavelength dependent terms in equations (4.1) and (3.5). We obtain for the figure of merit

$$F(\lambda_1,\lambda_2,E) = \frac{f(\lambda_1)-f(\lambda_2)}{f(\lambda_1)}\left[\frac{\lambda_1^4}{\eta_1\beta_1^2 R(\lambda_1)T_a^2(\lambda_1,E)} + \frac{\lambda_2^4}{\eta_2\beta_2^2 R(\lambda_2)T_a^2(\lambda_2,E)}\right]^{-\frac{1}{2}} \tag{5.4}$$

where $f(\lambda)$ is the wavelength dispersion term in the Marini-Murray atmospheric correction formula, η_1 and η_2 and β_1 and β_2 are the energy conversion efficiencies and pulsewidth reduction factors respectively for the relevant nonlinear process, $R(\lambda)$ is the spectral responsivity, and $T_a(\lambda, E)$ is the one way atmospheric transmission as a function of wavelength and elevation angle. The factor of λ^4 comes from the combined inverse square law dependence of the transmitter and target (retroreflector) gains on wavelength. The additional factor of λ associated with converting detector quantum efficiency to spectral responsivity cancels with a similar factor in (4.1) which converts transmitter laser energy to the number of transmitter photons. In plotting (5.4), we will use the envelope of the individual photoemitter responsivity curves in Figure 3 so that we present each wavelength in its most favorable light.

6 CONCLUSIONS

Figure 4 provides plots of the wavelength figure of merit as a function of the fundamental (laser) wavelength and elevation angle for the extremely clear atmosphere depicted in Figure 2. Parts (a), (b), and (c) correspond to elevation angles of 90, 45, and 20 degrees respectively. The three curves within each plot compare systems which use: (1) the fundamental and second harmonic wavelengths; (2) the fundamental and third harmonic wavelengths; and (3) the second and third harmonic wavelengths.

In spite of their greater dispersion, fundamental-third harmonic systems have the lowest figure of merit at all elevation angles due to a combination of poor detector performance at the fundamental and poor atmospheric transmission at the third harmonic. The performance of these systems peaks at a fundamental wavelength of about .97 microns independent of elevation angle.

At zenith, fundamental-second harmonic systems, operating at wavelengths of 670 and 335 nm, have the highest figure of merit (F = 1.75) but second-third harmonic systems, operating at wavelengths of 525 and 350 nm (fundamental = 1050 nm), are almost as good (F = 1.6). As one progresses to smaller elevation angles, atmospheric attenuation in the ultraviolet begins to dominate and the optimum fundamental wavelength is shifted toward longer wavelengths with a corresponding reduction in the wavelength figure of merit. Thus, the Nd:YAG laser, with a fundamental wavelength of 1064 nm and a very mature technology, is a near-optimum choice for a second-third harmonic system. However, a fundamental-second harmonic system which utilizes a Ti:Sapphire laser operating in the near infrared beyond 670 nm is a possible alternative.

Figure 5 suggests that a fundamental wavelength of about 400 nm is optimum for a hydrogen Raman-shifted laser and that these systems offer no real advantage over harmonic systems because of their lower wavelength figure of merit. This conclusion is further supported by the fact that there are no high power solid state lasers operating in the near ultraviolet. The principle short wavelength devices are excimer ("excited dimer") gas discharge lasers. At present, excimers cannot achieve ultrashort pulsewidths on the order of picoseconds, typically operate in the high atmospheric attenuation region of the spectrum below 360 nm, and are operationally less desirable than high power solid state lasers. Doubling or tripling solid state lasers to achieve a near ultraviolet wavelength prior to Raman shifting only decreases the overall wavelength figure of merit further by reducing the values for the energy efficiency factors η_1 and η_2. However, this effect is partially offset by the slight reduction in pulsewidth (increased β values) resulting from nonlinear generation.

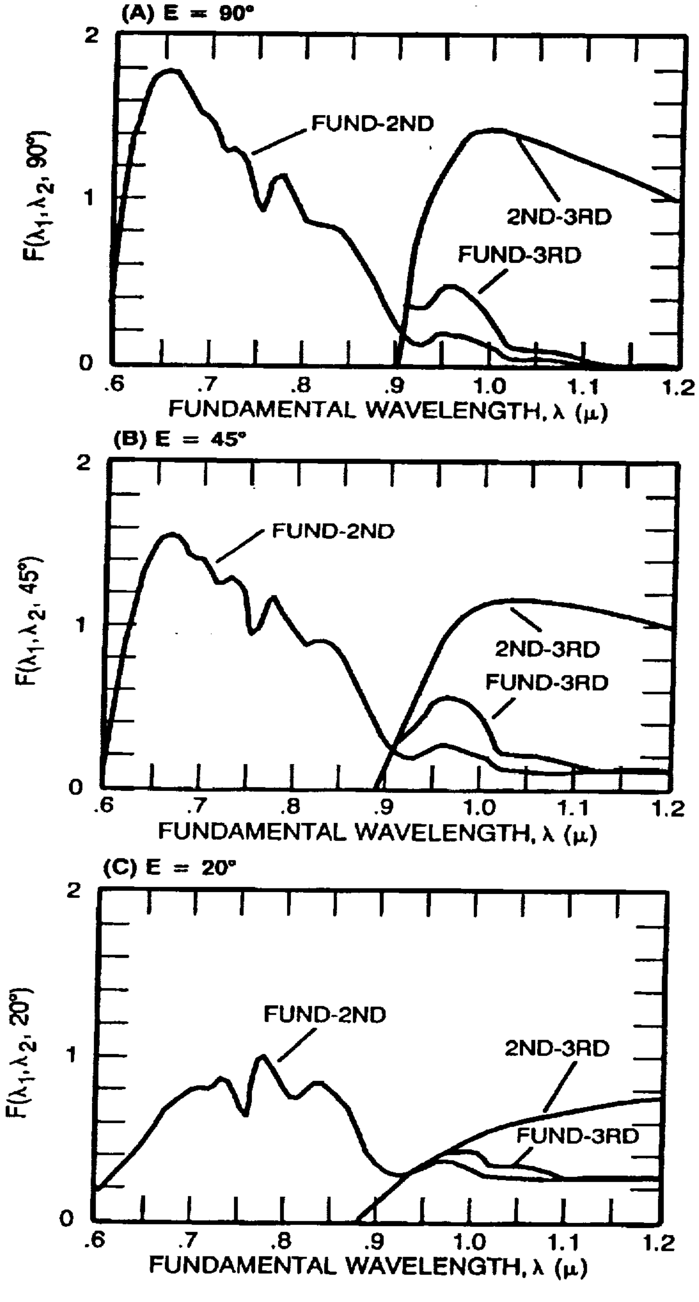

Figure 4. Two color wavelength figure of merit for fundamental-second harmonic, fundamental-third harmonic, and second-third harmonic systems operating in an extremely clear atmosphere at elevation angles of (a) 90°, (b) 45° and (c) 20° respectively.

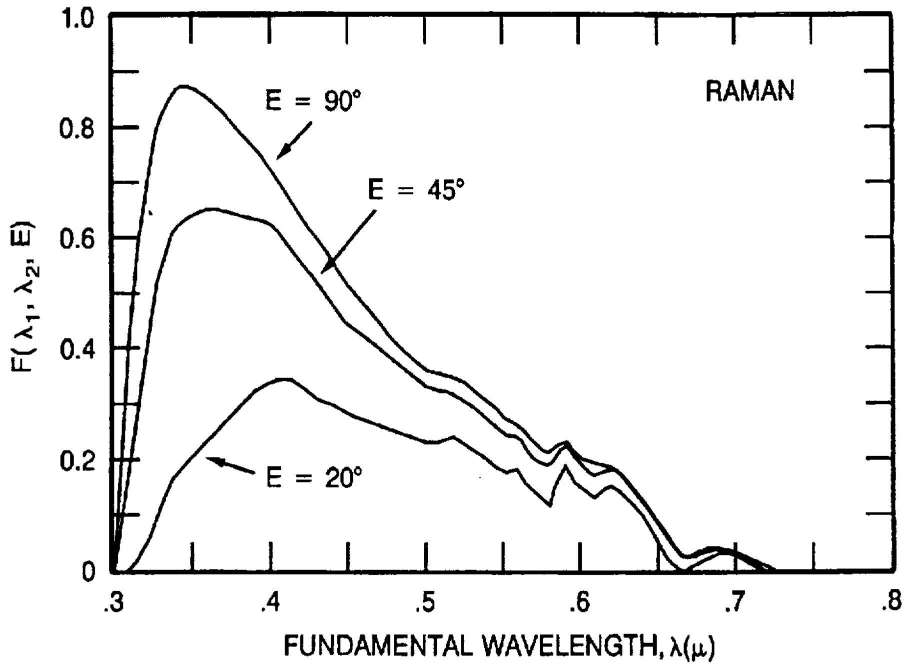

Figure 5. Two color wavelength figure of merit for Raman systems operating in an extremely clear atmosphere at elevation angles of 90^{o}, 45^{o} and 20^{o}.

7 REFERENCES

Abshire, J. B. and C.S. Gardner, "Atmospheric refractivity corrections in satellite laser ranging", IEEE Trans. on Geoscience and Remote Sensing, GE-23, pp. 414-425, 1985.

Degnan, J. J., "Physical processes affecting the performance of high-power, frequency-doubled short pulse laser systems: analysis, simulation, and experiment", Ph.D. Dissertation, University of Maryland, College Park, MD, May 1979.

Degnan, J. J., "Satellite Laser Ranging: Current Status and Future Prospects", IEEE Trans. on Geoscience and Remote Sensing, GE-23, pp. 398-413, 1985.

Degnan, J. J., "Millimeter Accuracy Satellites for Two Color Ranging", these proceedings (1992).

Gaignebet, J., F. Baumont, J. L. Hatat, K. Hamal, H. Jelinkova, and I. Prochazka, "Two wavelength ranging on ground target using Nd:YAG 2HG and Raman 0.68 μm pulses", Proceedings of the Sixth International Workshop on Laser Ranging Instrumentation, Antibes-Juan Les Pins, France, September 22-26, 1986.

Klein B. J., and J. J. Degnan, "Optical antenna gain. 1. Transmitting antennas", Applied Optics, 13, pp. 2134-2140, 1974.

Marini, J. W. and C. W. Murray, "Correction of laser range tracking data for atmospheric refraction at elevations above 10 degrees", NASA Report X-591-73-351, Goddard Space Flight Center, 1973.

Owens, J. C., "Optical refractive index of air: Dependence on pressure, temperature, and composition", Applied Optics, 6,51-58, 1967.

RCA Electro-optics Handbook, Technical Series EOH-10, RCA Commercial Engineering, Harrison, NJ, 1968.

Slater, P. N., Remote Sensing: Optics and Optical Systems, Chapter 13, Addison-Wesley Publishing Co., Reading, Massachusetts, 1980.

Zwicker, H. R., "Photoemissive Detectors", in Optical and Infrared Detectors, Ed. R. J. Keyes, Springer Verlag, New York, 1977.

N94-15581

Two Color Satellite Laser Ranging Upgrades At Goddard's 1.2m Telescope Facility

Thomas W. Zagwodzki
Jan F. McGarry
John J. Degnan

NASA/Goddard Space Flight Center
Greenbelt, Maryland 20771

Thomas K. Varghese

Bendix Field Engineering Corporation
Seabrook, Maryland 20706

Abstract

The ranging laboratory at Goddard's 1.2m telescope tracking facility has recently been upgraded to include a single photoelectron sensitive Hamamatsu streak camera-based range receiver which uses doubled and tripled Nd:YAG frequencies for satellite laser ranging. Other ranging system upgrades include a new Continuum laser, which will deliver up to 30 millijoules (mJ) at both 532 and 355 nm at a pulsewidth of 30 picoseconds (FWHM), and replacement of both ranging and tracking computers with COMPAQ 386 based systems. Preliminary results using a photomultiplier tube based receiver and waveform digitizer indicate agreement within the accuracy of the measurement with the theoretical Marini and Murray model for atmospheric refraction. Two color streak camera measurements will be used to further analyze the accuracy of these and other atmospheric refraction models.

INTRODUCTION

Satellite laser ranging efforts at the 1.2m tracking telescope at Goddard's Geophysical and Astronomical Observatory (GGAO) have evolved over the past few years in response to the demand for more accurate SLR data. This includes a frequency-tripled Nd:YAG laser system and a streak camera based range receiver. The laboratory which houses the Experimental Satellite Laser Ranging System (ESLRS) adjoins a azimuth-elevation mount multi-user facility designed to support the scientific community at the Goddard Space Flight Center. Two of six facility experimenter port locations are dedicated to the laser transmitter and the streak camera based receiver for ranging applications. The ESLRS is a ranging laboratory where new instrumentation, hardware and software are investigated and characterized for planning and developing next generation systems. The SLR data gathered by the ESLRS is considered engineering data and is not archived as is other NASA laser tracking network data. The end users of the ESLRS data are the experimenters and their goal is to use this information to better understand system problems and to help transition laboratory systems more efficiently to field SLR operations. Other system upgrades include a new 386 based tracking computer, a new 386 based ranging computer, and physical plant upgrades at the facility.

The ESLRS has been operational since 1983 except for periods in which high priority flight programs within the Instrument Electro-Optics Branch left the facility without crew support. The initial SLR system [McGarry et al, 1986] included a Quantel YG 402 DP frequency-doubled Nd:YAG laser, a two stage ITT F4128 microchannel plate photomultiplier tube (MCP-PMT), Ortec 934 and later Tennelec TC 453 constant fraction discriminators (CFD's), and a developmental time interval unit (TIU) built by Lawrence Berkeley Laboratory. This system operated at a 5 hertz rate at the doubled YAG wavelength (532nm) and yielded data at the 1 to 2 centimeter level on LAGEOS with a very high return-to-fire ratio.

PROGRAM GOALS

Goddard Laser Tracking Network (GLTN) systems currently operating at or below the 1 cm level RMS must still rely on models of atmospheric range correction which assume certain altitude profiles for temperature, pressure, and possible gradient effects. Knowledge of atmospheric range correction on a shot-to-shot basis is therefore uncertain, and must be addressed to eliminate atmospheric concerns. The best way of accounting for the atmospheric range correction is to measure it on a shot-to-shot basis. The time of flight measurement is made in the conventional manner with a MCP based receiver using the 532nm pulse, while a differential time of flight between the 532nm and 355nm pulses is made with a streak camera based receiver. In making a streak camera differential measurement accurate at the few picosecond level, the atmospheric range correction can be recovered at the few millimeter level. Work in improving ground-based SLR accuracies closely parallel work on planned next generation space-based laser ranging systems. Efforts in the ranging laboratory at the 1.2m facility have been concentrating on both programs in this parallel effort.

SYSTEM UPGRADES

The extension from single color to two color operation at the 1.2m facility required significant system upgrades, one being an improvement in low mirror reflectivities in the UV. Recoating of all telescope mirror surfaces was required since previous coatings revealed mirror reflectivities in the UV of typically 50 to 60% and one as low as 40%. For a 6 mirror coude focus system used in common optics configuration, UV operation was prohibitive. New aluminum mirror coatings with an SiOx overcoating (peaked at 355nm) improved surface reflectivities to typically 92% at 355nm and 88% at 532nm while maintaining broadband characteristics required by other experimenters at the facility.

Return signal levels from LAGEOS are not adequate for two color streak camera-based operation with the present system. Therefore we have opted to use low earth orbiting satellites such as STARLETTE, AJISAI, and ERS-1 for two color data collection. As an acquisition aid for sunlit passes, two TV camera systems have been added to the mount, and a third low light level RCA silicon intensified target (SIT) camera has been used in the system prime focus.

Facility upgrades include the replacement of the PDP 11/24 tracking computer with a COMPAQ 386/20 based system, and new meteorological instruments including air pressure, temperature, and relative humidity. The ranging computer, a LSI 11/23 (MINC), was also replaced with a COMPAQ 386/20 system.

Ranging instrumentation upgrades include both laser transmitter and receiver. The laser available for use at the 1.2m facility for ranging from 1983 to March of 1992 was a Quantel passively mode locked Nd:YAG system model number YG402 DP. This laser system generated up to 60 mJ of doubled YAG at 532nm and about 15 mJ of tripled YAG at 355 nm in a 140 picosecond pulse (FWHM). To make differential measurements accurate at the picosecond level laser pulsewidths must be narrowed considerably, and target satellites with low pulse spreading must be used. The Quantel laser was replaced with a Continuum model PY-62 YAG with doubling and tripling capability. The new Continuum laser outputs 30 picosecond pulses with about 30 mJ of energy at both 532nm and 355nm. The laser fire rate is currently 4 hertz, with work underway to increase it to 10 hertz.

The laser is housed in a clean room approximately 10 meters from the base of the mount. The output beam is coupled into the telescope system with a negative lens (negative focal length matching the F28 ray bundle of the 1.2m system) and a 45 degree aperture sharing 'holey' mirror just inside the system focal plane. The outgoing laser beam is translated approximately 1.25 cm from the optical axis of the telescope to avoid the shadowing by the central obscuration (secondary mirror) in the telescope. The output beam is approximately .4m in diameter, exits the system cleanly between the primary and secondary mirror, and travels around that annulus as the system tracks in azimuth. This configuration results in the least amount of loss in the outgoing beam. In the common optics mode the return path at the 45 degree mirror is folded across an NRC table top to another mirror, splitter, and receiver package. In the prime focus of the system is a field stop, to limit the receiver field of view, and a high speed shutter.

The receive signal is split between a two stage ITT model F4128 MCP PMT and a Hamamatsu streak camera. Shown in Figure 1 is a simplified block diagram of the system that was used for both aircraft and Relay Mirror experiments as well as current SLR activities. The streak camera in use up until the Spring of 1992 was

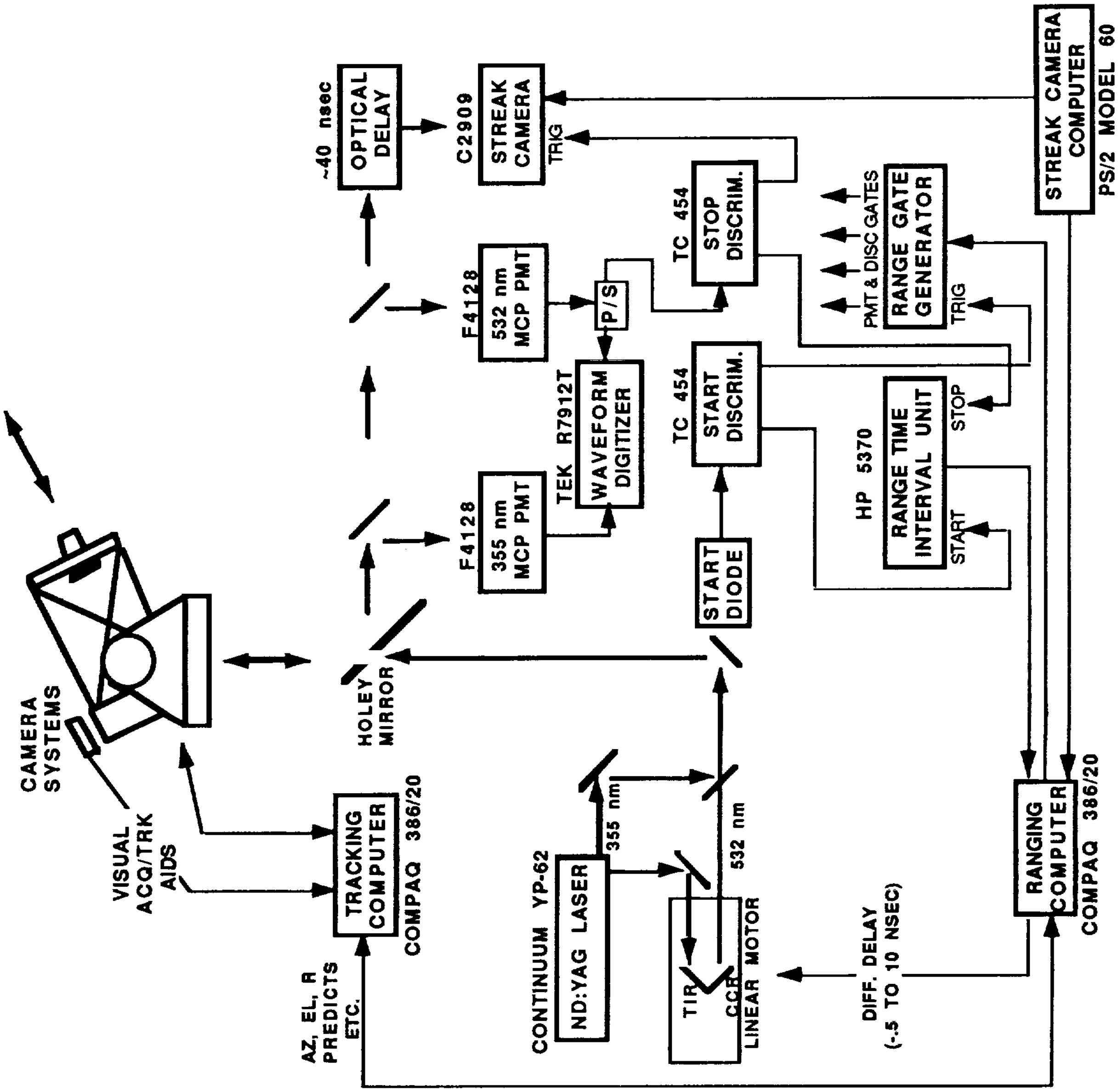

Figure 1. Two Color SLR Simplified Block Diagram

a 2 picosecond resolution Hamamatsu model 1370. This unit was integrated into the system in support of two color experiments which included both aircraft and the NASA/Air Force Relay Mirror Experiment (RME) programs. The signal threshold for the Hamamatsu 1370 streak camera is estimated at several thousand photoelectrons and could be used only for ground work, aircraft, and the RME program where signal levels were extremely high. The Hamamatsu 1370 streak camera has since been replaced with a newer Hamamatsu model 2909 which has an additional internal microchannel plate intensifier giving the unit single photoelectron sensitivity. A summary of upgraded system parameters is given in Table 1.

Table 1. Laser Ranging System Parameters and Instrumentation

Laser	Continuum PY-62, active/passive mode-locked	
Energy	30 mJ @ 532 nm, 30 mJ @ 355 nm	
Pulsewidth	30 picoseconds (FWHM)	
Beamwidth	.0057 degree (FWHM)	
Telescope	1.2 meter diam., f/28 Cassegrain Common optics configuration	
Trans/Rec Sw	Aperture shared	
System trans	60%	
Detector	ITT F4128 MCP PMT	
Discriminator	Tennelec TC 454	
Time Interval Unit	HP5370, 20 ps resolution	
Streak Camera	Hamamatsu model 2909	
Minicomputers	COMPAQ 386/20:	Tracking
	COMPAQ 386/20:	Ranging
	PS/2 model 60:	Streak camera

In the ranging mode a small fraction of the return signal is detected with the MCP PMT, discriminated with a CFD, and triggers the streak camera sweep. Both streak cameras require a pretrigger of 25 to 40 nanoseconds dependent on the sweep speed selected. Sweep speeds available in both cameras are .3, 1, 2, 5, and 10 nanoseconds full scale. The pretrigger is accomplished by delaying the optical return by one of two means. The streak camera input signal is delayed with either a white cell optical delay, or a spot to slit 10m multimode fiber optic bundle. Each technique has it's own advantages and disadvantages. The fiber optic bundle is easy to align and has the largest field of view, but introduces pulse spreading, while the white cell has the best throughput, no pulse spreading, but is difficult to align. To maintain the best differential timing capability at the receive end an artificial delay on the 532nm pulse is introduced at the laser transmitter. This delay is a dogleg optical path into a total internal reflection (TIR) cube corner on a Compumotor linear motor stage. The linear translation stage provides the differential delay control from -.5 to 10 nanoseconds additional optical path length for the 532nm pulse so that both return pulses can be maintained within the 1 nanosecond sweep window. The linear motor stage under computer control uses the differential delay predicted by differencing the Marini & Murray model delays at 355nm and 532nm The optical delay is adjusted so that the two spatially separated pulses are incident in the streak camera slit at approximately the same time. This minimizes nonlinearity problems in the streak camera sweep. To resolve simultaneous pulses in the PMT based receiver using the waveform digitizer two PMT'S must be used.

PRELIMINARY RESULTS

The NASA/Air Force two color RME experiment mentioned earlier generated the first streak camera returns for the ESLRS [Zagwodzki et al, 1992]. The RME satellite was very attractive for several reasons. The RME satellite represented an active, single cube corner response target with an extremely high lidar cross section (~6×10^9 m^2). With a short pulse laser transmitter and streak camera based receiver, the individual cube corners on the satellite, separated by 41.2 mm, could be resolved in time. In the Fall of 1991 the only streak camera available at the 1.2m facility for the RME program was the Hamamatsu model 1370. The high threshold of several thousand photoelectrons for this streak camera made the RME the only viable satellite target. Shown in Figure 2 are streak camera return waveforms from the RME satellite at 532nm only. Three cube corners on the satellite could clearly be resolved in time (separation of 41.2mm). The horizontal sweep speed was 1.2 nanoseconds in time and the laser pulsewidth was 140 picoseconds. Unfortunately satellite control problems ended the experiment prematurely before UV operation began.

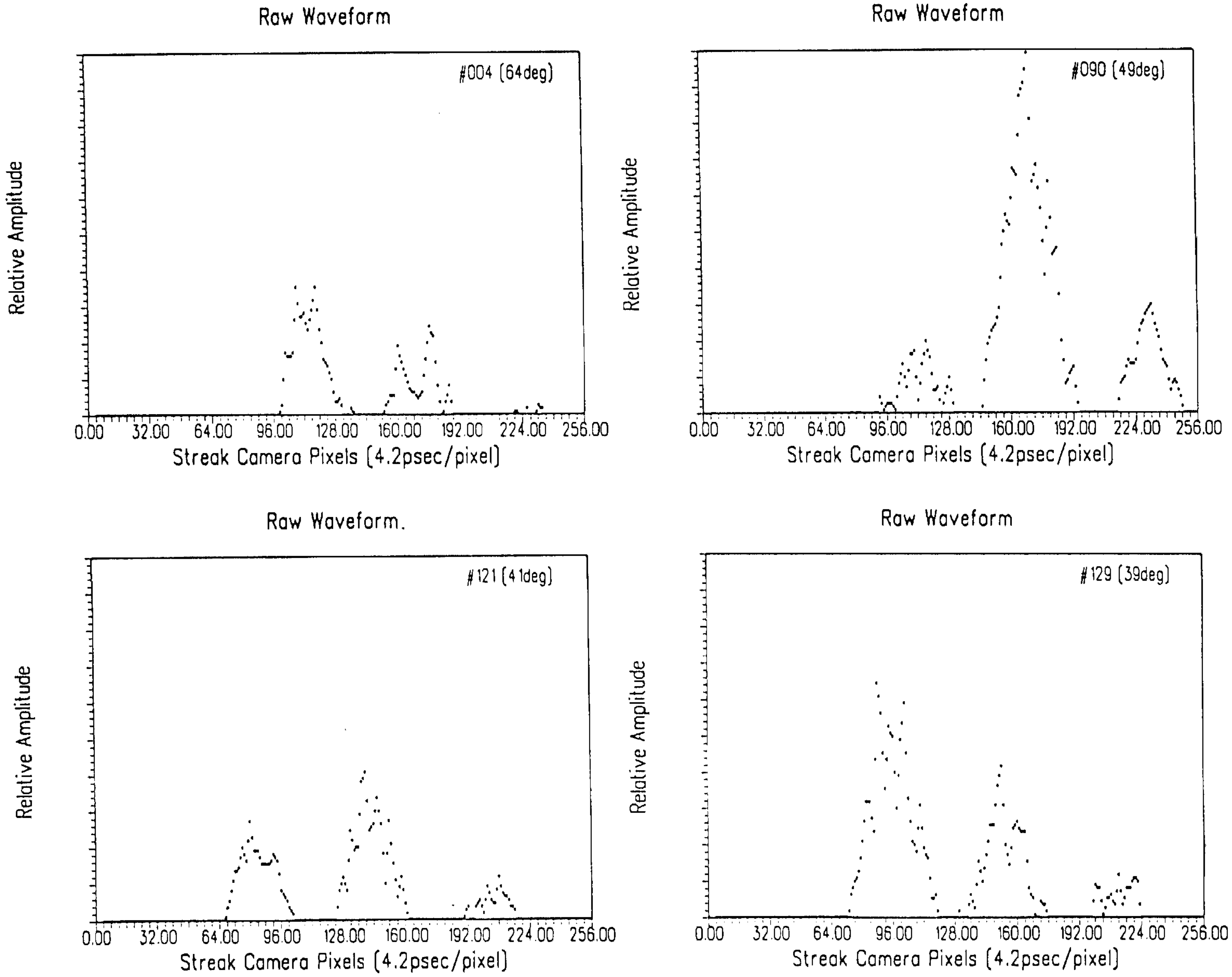

Figure 2. 532nm streak camera returns from the RME

The loss of the RME as a target meant satellite streak camera work had to wait for the installation of the more sensitive Hamamatsu 2909 unit. In the interim, two color efforts have continued at the 1.2m facility using the MCP PMT based receiver with a 1 Ghz bandwidth Tektronix model 7912 waveform digitizer. The ranging system can be configured with two PMT's (one each for 532nm and 355nm) or a single PMT (usually the 355nm). For night time operation, when no bandpass filters are required, a single PMT is used. Since the UV link is the weakest, the PMT with peaked quantum efficiency at 355nm is used. To resolve two distinct pulses with the single UV PMT the differential delay at the transmitter is set to allow at least two nanoseconds offset between the peaks of the two pulses. This assures adequate separation of return pulses at the receiver, but reduces the temporal resolution of the differential time-of-flight measurement.

Figure 3 shows a comparison plot of the theoretical differential delay versus the measured delay calculated from the two color returns as seen by the Tektronix 7912. The theoretical differential delay was calculated by differencing the 355nm and 532nm delays computed using the Marini and Murray model. The Marini and Murray calculations used the weather conditions from the log file taken during the pass. This weather information was taken in real-time, so the actual temperature and pressure were not constant. The pressure changed minimally (1006.27 to 1006.31 millibars) as did the temperature (14.24 to 14.48 C). The gaps (thinner lines) in the Marini and Murray curve represent times that no weather information was available, and so the data had to be interpolated for those regions.

For this pass the linear translator was fixed at 6 nanoseconds. This necessitated a slow sweep setting on the 7912 waveform digitizer in order to capture both frequency's return waveforms during the entire pass. Setting the green delay at 6 nanoseconds always placed the 355nm return ahead of the 532nm return and caused the UV pulses to move toward the green as the elevation decreased.

The measured differential delay was computed by taking the inverted raw 7912 waveforms (no smoothing) and computing the pixel locations of the highest two peaks. The location of these two pixels was differenced, converted to nanoseconds, and subtracted from the fixed 6 nanosecond green delay. This was a "quick-look" at the data so no interpolation was performed between pixels, and

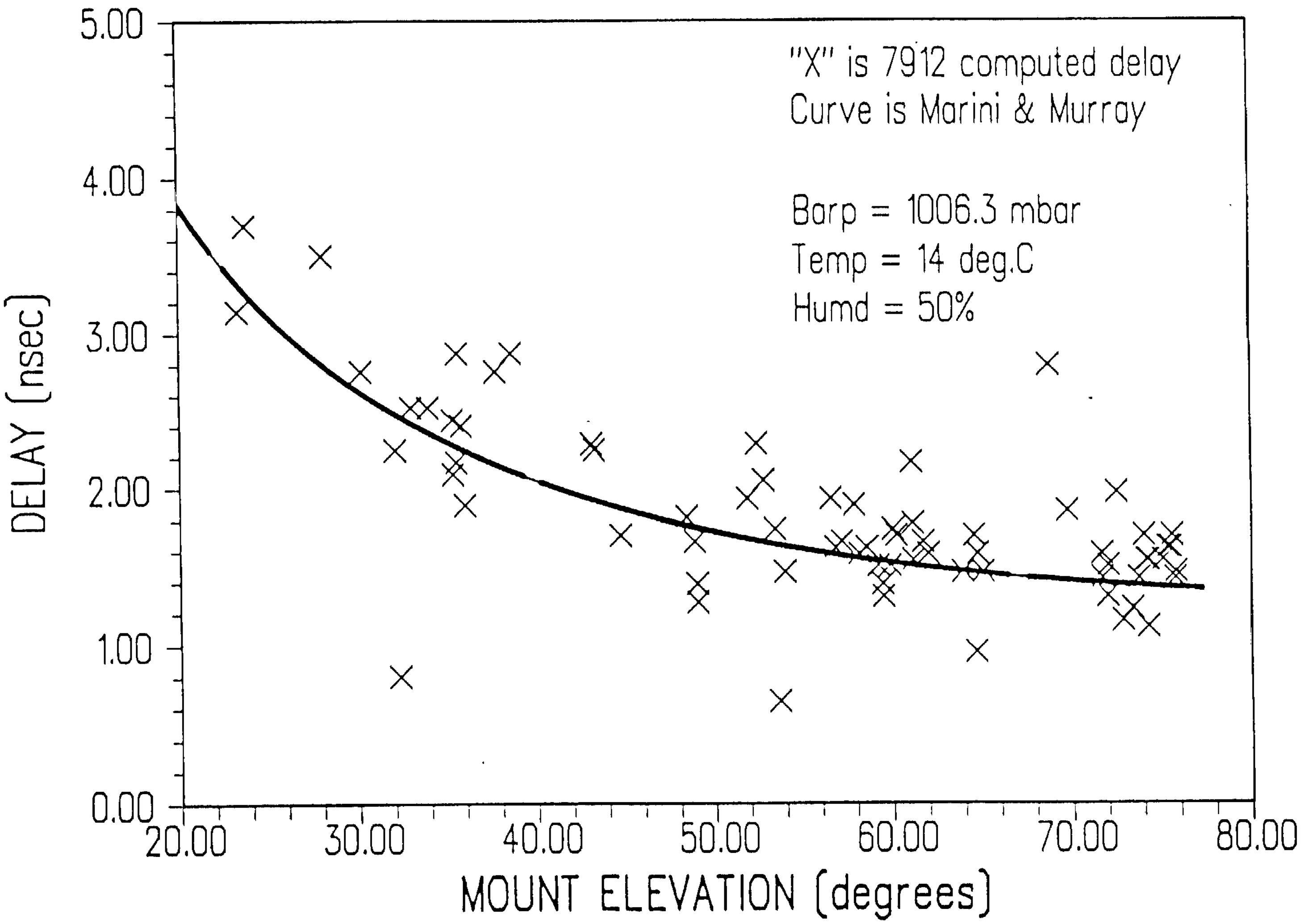

Figure 3. Two color differential delay comparison of AJISAI pass of June 27, 1992.

there was no 7912 calibration data used to correct any nonlinearities in the sweep.

The calibration of the linear translator was not performed as accurately as it will be for streak camera data. The actual zero point of the translator for the 7912 data was good to approximately +/- 200 picoseconds. Actual raw 7912 return waveforms at different elevations are shown in Figure 4. In these plots the 7912 data is inverted, but not smoothed in any way.

FUTURE WORK

Two color laser ranging activities will continue at the 1.2m facility to complete the installation of the streak camera based receiver with single photoelectron sensitivity. This will enable tracking of all low earth orbit satellites in two colors and will yield a good data set for atmospheric model comparisons. Investigative work will begin in the areas of system automation, and optical time interval units. [Degnan, 1985]

ACKNOWLEDGEMENTS

The authors wish to thank the Strategic Defense Initiative Organization Office of Directed Energy for use of the Relay Mirror Experiment satellite, the Phillips Laboratory of Albuquerque, New Mexico for their coordinating efforts, and the Consolidated Space Test Center of Sunneyvale, California for their work in providing NASA the satellite maneuvers for optical engagements.

We would like to thank Arnie Abbott of NASA for his services in maintaining the 1.2m facility, and Tammy Bertram for her operational support. We would also like to thank Bendix Field Engineering Corporation crew members Dick Chabot, Jim Fitzgerald, Dave Grolemund, Mike Seldon, Tom Oldham, and Jack Cheek of Hughes- STX for their continued effort in support of this program.

REFERENCES

J.J. Degnan, "Satellite Laser Ranging: Current Status and Future Prospects", IEEE Trans. on Geoscience and Remote Sensing, GE-23, pp. 398-413, July, 1985.

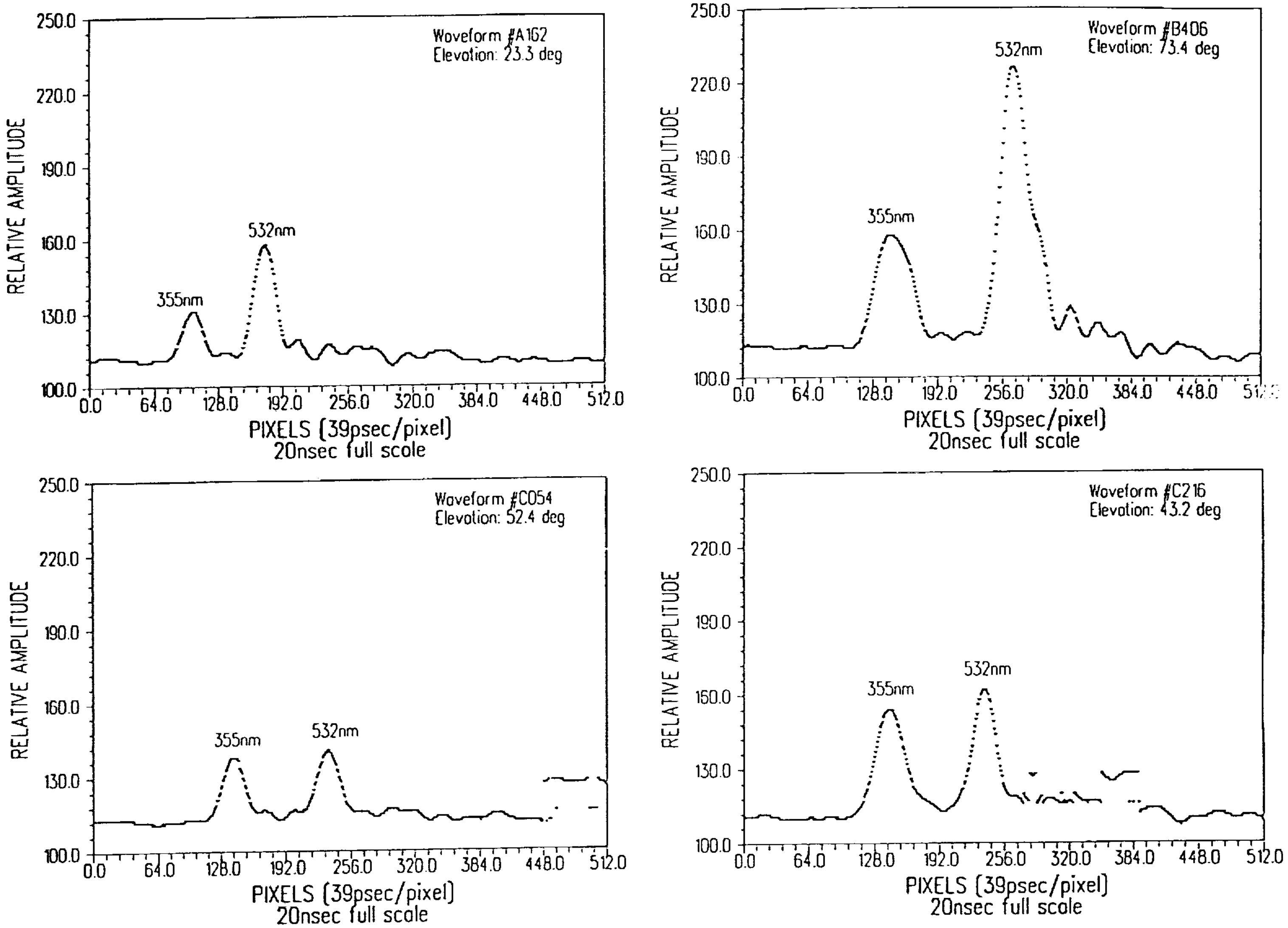

Figure 4. Two color return waveforms from AJISAI pass of June 27, 1992.

J. L. McGarry, T. W. Zagwodzki, J. J. Degnan, "Large aperture high accuracy satellite laser tracking," in Proc. of S.P.I.E. Acquisition, Tracking, and Pointing, Orlando, Florida, April, 1986.

T.W. Zagwodzki, J.F. McGarry, A. Abbott, J.W. Cheek, R.S. Chabot, J.D. Fitzgerald, D.A. Grolemund, "Laser Ranging to the Relay Mirror Experiment (RME) Satellite from Goddard Space Flight Center's 1.2m Telescope Facility", to be published in the *Journal of Geophysical Research*.

N94-15582

Measuring Atmospheric Dispersion With WLRS In Multiple Wavelength Mode

U. Schreiber[1]
Forschungseinrichtung Satellitengeodaesie
Fundamentalstation Wettzell
D - 8493 Koetzting

K. H. Haufe R. Dassing,
Institut fuer Angewandte Geodaesie
Fundamentalstation Wettzell
D - 8493 Koetzting

Abstract

The WLRS (Wettzell Laser Ranging System) allows the simultaneous tracking of satellites on two different wavelengths. These are the fundamental frequency of Nd:YAG at 1.064 μm and the second harmonic at 532 nm. Range measurements to the satellite LAGEOS were carried out with different experimental set- ups, after developing a detector unit based on a silicon avalanche photodiode in Geiger mode, which is sufficiently sensitive in the infrared domain. An approach towards a quantitative interpretation of the data is suggested and discussed briefly.

1 The effect of atmospheric dispersion on satellite ranges

The varying index of refraction of the atmosphere can be considered one of the most important contributions to the error sources for satellite ranges. Following a model of Marini and Murray [1], the additional time for the laser pulse passing through the atmosphere under an elevation angle of 90 degrees is as much as 8 ns. This model assumes rotational symmetric atmospheric layers with respect to the geocenter and has been established with the help of ballon experiments. Inputs to to this model are atmospheric pressure, temperature and humidity, which are measured around the ranging station. In general it can be said that the calculated corrections are very precise, so that the requirements for an experimental improvement are extremly high [2]. However, orbit fitting procedures on the basis of complex programs often show a small systematic error, depending on the pointing elevation of the ranging station. Therefore a better determination of the atmospheric influence is desirable.

2 The experimental set- up

2.1 The 'two-' detector experiment

When the WLRS telescope was designed [3], care had been taken to optimise the signal path for the fundamental (1.064 μm) and second harmonic (532 nm) wavelength of the Nd:YAG

---

[1] Techn. Universitaet Muenchen, Arcisstr. 21 D - 8000 Muenchen 2

laser. The remaining optical components of the ranging equipment were replaced to allow transmission and reception of these 2 frequencies. In the beginning it was not known if the second harmonic generating crystal (KD^*P) would laterally displace the pulses of the 2 frequencies so far, that there would not be a sufficient overlap of the two signals at the location of the satellite. During the experiments a weak dependance of the return rate of each detector with respect to the pointing was noticed. However, the overlap was found to be acceptable. The WLRS- system uses the same telescope for transmitting and receiving, therefore the photodetector was placed behind the transmit/receive- switch inside the thermocontrolled laboratory. This gives the advantage of high signal stability and an easily accessible working enviroment. Figure 1 outlines the experimental set- up. The receive signal is split into its two different frequency components at a dichroic mirror. The signal with a wavelength of 532 nm is reflected towards a microchannel plate (MCP), while the infrared part of the satellite echo is focused onto the active area of an avalanche photodiode (APD: SP114) placed in Geiger mode. In its present state, the WLRS is capable of recording one stop event per outgoing laser pulse only. This causes the detection of either an event from the MCP or the APD. To achieve a high number of echos from both channels, a constant delay- line of 44.9 ns was added to the MCP output, before recombining both signal lines at an impedance matched T - junction and feeding them to the eventtimer. There are two stops for each measured roundtrip possible, only one of them will be recorded, as the electronics gets disactivated after processing one event. The delayline places the less favourable signal channel to be detected first. When the measured return residuals are plotted versus time one can see two signal tracks (fig. 2) separated in range by the delay of the additional cable. This can be noticed during tracking and indicates, if there are enough recordings for both laser frequencies. The contribution to each wavelength has to be separated during the analysis, as all the range information goes to one datafile.

2.2 The 'one-' detector experiment

A slowly varying instability (i.e. drift) in the detector characteristics would be indicated during the ranging run, as a shot by shot calibration to a fixed target is carried out. To exclude such effects generally, the experiment was altered to use just one detector. The dichroic mirror (ref. fig. 1) was removed and the APD recorded both frequencies. The sensitivity of the diode is higher on 532 nm than on 1.064 μm but, because of the dispersion of the atmosphere, the infrared signal reaches the detector first. Therefore, a sufficient amount of data for both signal frequencies can be obtained. For the present this kind of experiment is restricted to the night hours, as there are no suitable spectral filters for this application. During tracking, the operator notices the formation of one track only, as both satellite tracks are separated by their differential atmospheric dispersion delay only, which contributes as much as 0.6 to 1.8 ns. In figure 3 there is a residual plot for such a measurement. In the analysis the two tracks also have to be seperated. To calibrate this measurement a circuit has been developed, which detects the starting oscillation in the laser after the fire command and forms a trigger signal to gate the APD into the Geiger mode before the calibration return hits the diode. This process is extremly time critical. Measurements to the local ground target demonstrate the proper operation of this set- up.

3 Analysing the satellite data

In this approach the question of wether the simultaneous use of different laser frequencies would result in the same satellite range information and, under the condition that a large amount of ranges have been measured, whether the measurements would allow for a correction of the employed atmospheric model were of interest. Therefore the analysis is limited to the differences in the range residuals of the two spectral components. In the following, the measurements obtained at a wavelength of 532 *nm* are taken as a reference to correct for other satellite ranging side effects; a non linear least squares fitting procedure is employed to fit a polynomial up to the order of 12 to the reference data. In the second step, the range residuals of the measurement in the infrared spectral domain are analysed. It was assumed that this data can be represented by the same polynomial when the additional contribution by the atmospheric dispersion and, if applicable, the extra cable delay is taken into account. Under the condition that the model of Marini and Murray gives a good representation of the atmospheric influence, so that there can be a minor modification to it only, it is:

$$r(t)_{\lambda=1.064\mu m} = r(t)_{\lambda=532nm} - \alpha\mathcal{M}(\omega) - \beta,$$

where $\mathcal{M}$ represents the contribution of the difference of the atmospheric dispersion of the two used laser frequencies depending on the elevation angle ω. α is a dimensionsless scaling factor around the value of 1 and β yields the constant value of the introduced extra delay. The measured range depending on the epoch is given by r. A curve fitting result of $\alpha = 1$ gives the exact representation of the Marini- Murray model. It is a known fact that a possible range correction for this pair of frequencies contributes with a value of only a few *ps* to the difference between the two used laser frequencies at a given pointing elevation (i.e. a fixed pathlength through the dispersive medium). This can not be taken from the range residual distribution. However, the characteristic elevation dependence of the difference of the ranges of the two laser frequencies places a constraint on the model, such that it might allow an interpretation of the ranging results, especially when a wide range of elevation angles has been spanned by the measurements. At low elevation angles, the separation of the two frequency components is largest, so it is desirable to range down to very low elevation angles. The model has been tested by creating a data set, introducing $\alpha = 1.05$ to an arbitrarily chosen data set of ranges artificially. After running through the evaluation procedure $\alpha = 1.05002$ was obtained as a result. This shows, that a small additionally introduced effect could be well extracted by this procedure. However, this can not be taken as sufficient proof for the applicability of the suggested model modification.

4 The experimental results

Up to now there are two series of measurements, one for each experimental set- up. In figures 4 and 5 the obtained range residuals are plotted versus the angle of elevation. In the lower part of each diagram the fitted data of the reference wavelength ($\lambda = 532$ *nm*) is displayed, while the upper half shows the satellite returns taken at the other laser frequency. In all cases a satisfying residual distribution around the fitted curve was obtained. As a side effect, figure 5 shows a higher sensitivity of the photodiode in the infrared spectral range. This was unexpected because the system is at least one order of magnitude more sensitive around 532 *nm*. The results are summarized in table 1:

Date:	Type	α	$\beta[ns]$
4. Oct. 91	MCP/APD	0.92	44.89
8. March 92	APD	1.02	-0.027

Table 1: The results of the parameter fitting procedure of the 2 LAGEOS passages

In both cases a good representation of the expected contribution of the second laserpulse with a different wavelength was obtained. The passage of LAGEOS, measured in Oct. 1991, shows a small offset from the Marini- Murray formula, but , it is beyond the point of interpretation within the frame of this work. More experience with this measurement technique and much more data are necessary to judge the applicability of this approach. A higher resolution in the measurement of the satellite ranges is also desirable. Therefore, a modification of this experiment using a streak camera is in preparation. The goal is a higher precision in measuring the time difference in the roundtrip between the two spectral components simultaneously. Furthermore, the measurements will be extended to lower elevation angles and the search for APD's with less jitter and noise will also be continued.

Summarizing the present state of the simultaneous ranging on two different laser pulse frequencies, one can say that the obtained ranges under normal atmospheric conditions do not depend on the wavelength of the employed laser.

References

[1] Marini, J. W.; Murray, C. W.; *Correction of Laser Range Tracking Data for Atmospheric Refraction at Elevations above 10 Degrees* NASA X- Document 591-73-351 (Nov. 1973)

[2] Abshire J. *Pulsed multiwavelength laser ranging system for measuring atmospheric delay* Aplied Optics / Vol. 19, No. 20 / 15 October 1980

[3] Schlueter, W.; Hauck, H.; Dassing, R.; Schreiber, U.; Mueller, J.; Egger, D.; *Wettzell Laser Ranging System (WLRS) — First Tracking Results to Satellites and to the Moon, paper presented at the Crustal Dynamics Project Meeting, held in Pasadena, spring 1991.*

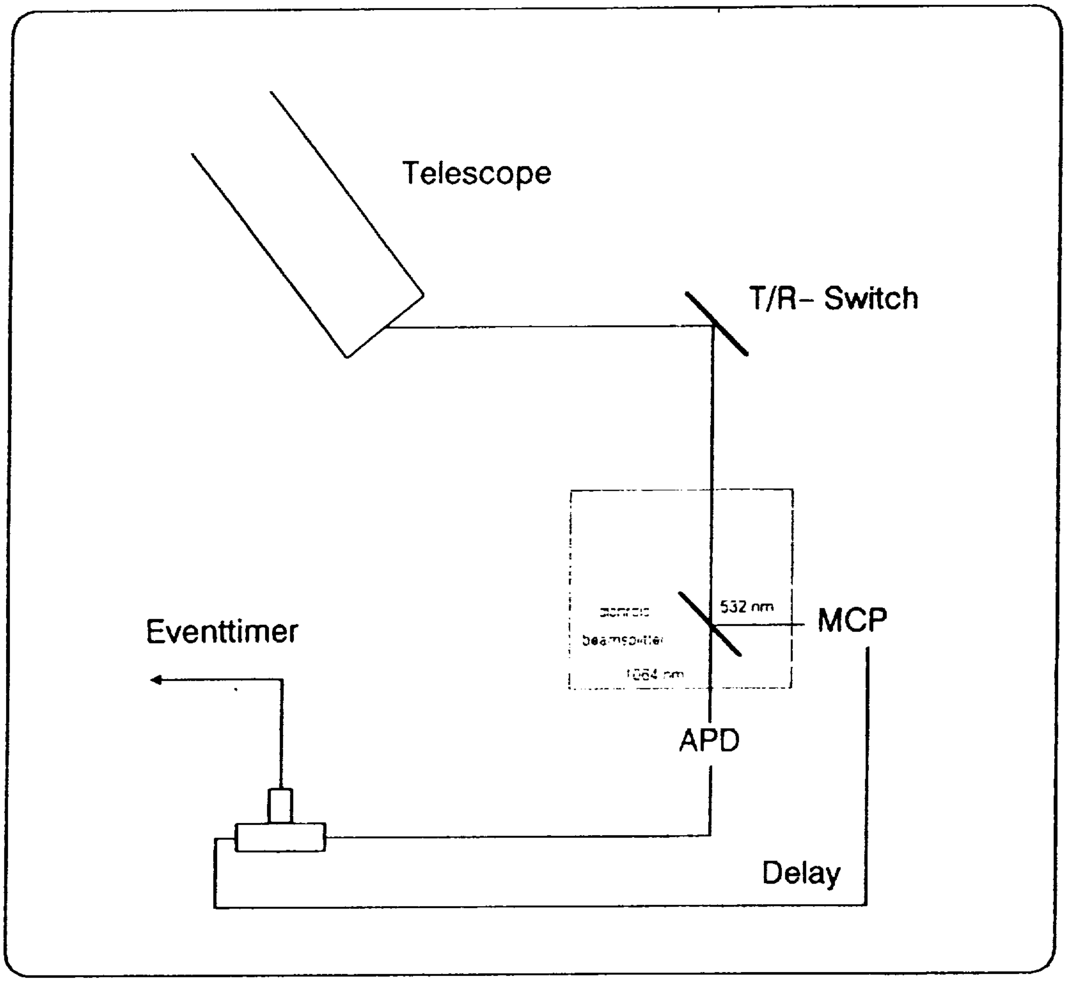

Figure 1: Block diagram for the two detector set- up

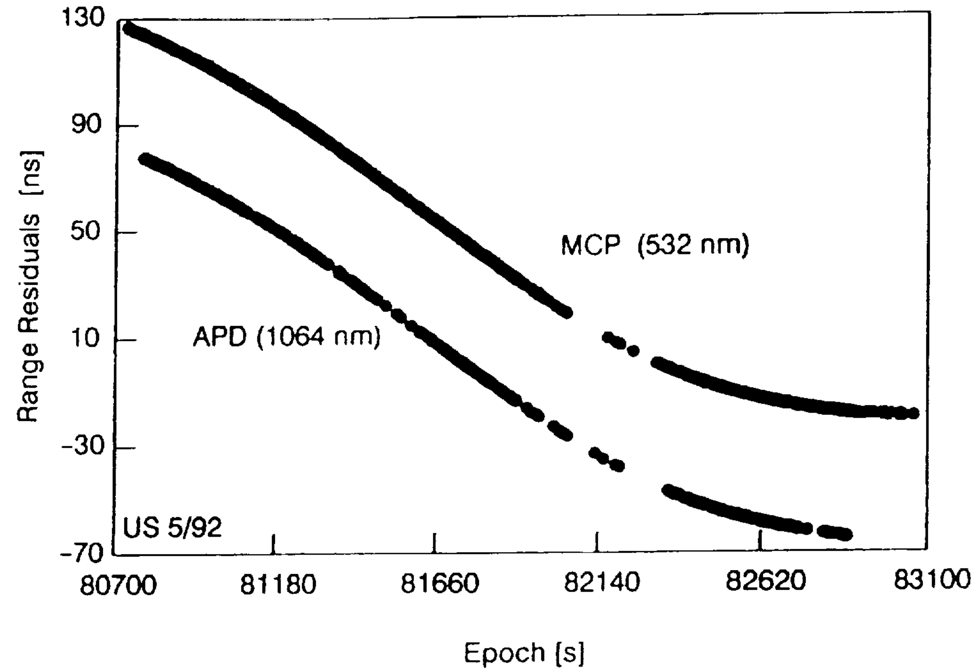

Figure 2: Residual plot of the measured LAGEOS pass from Oct. 4th 1991 after the screening process. The lower track was recorded using the Avalanche photodiode SP114, while the upper track was obtained using a microchannel plate ITT: F 4129 f

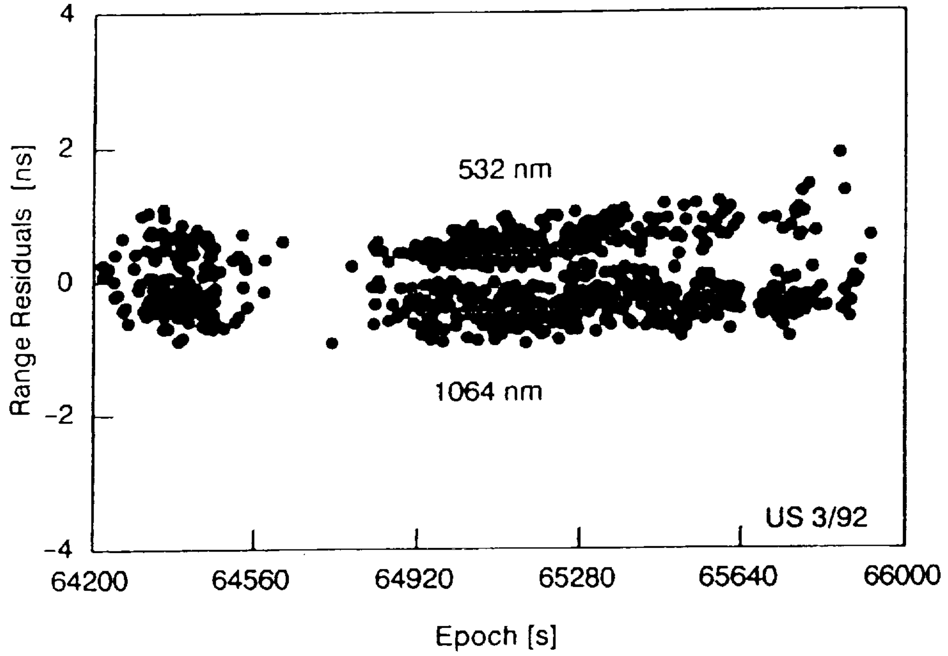

Figure 3: Residual plot of the measured LAGEOS pass from March 8th 1992 after the screening process. Both frequency components were recorded, using the Avalanche photodiode SP114

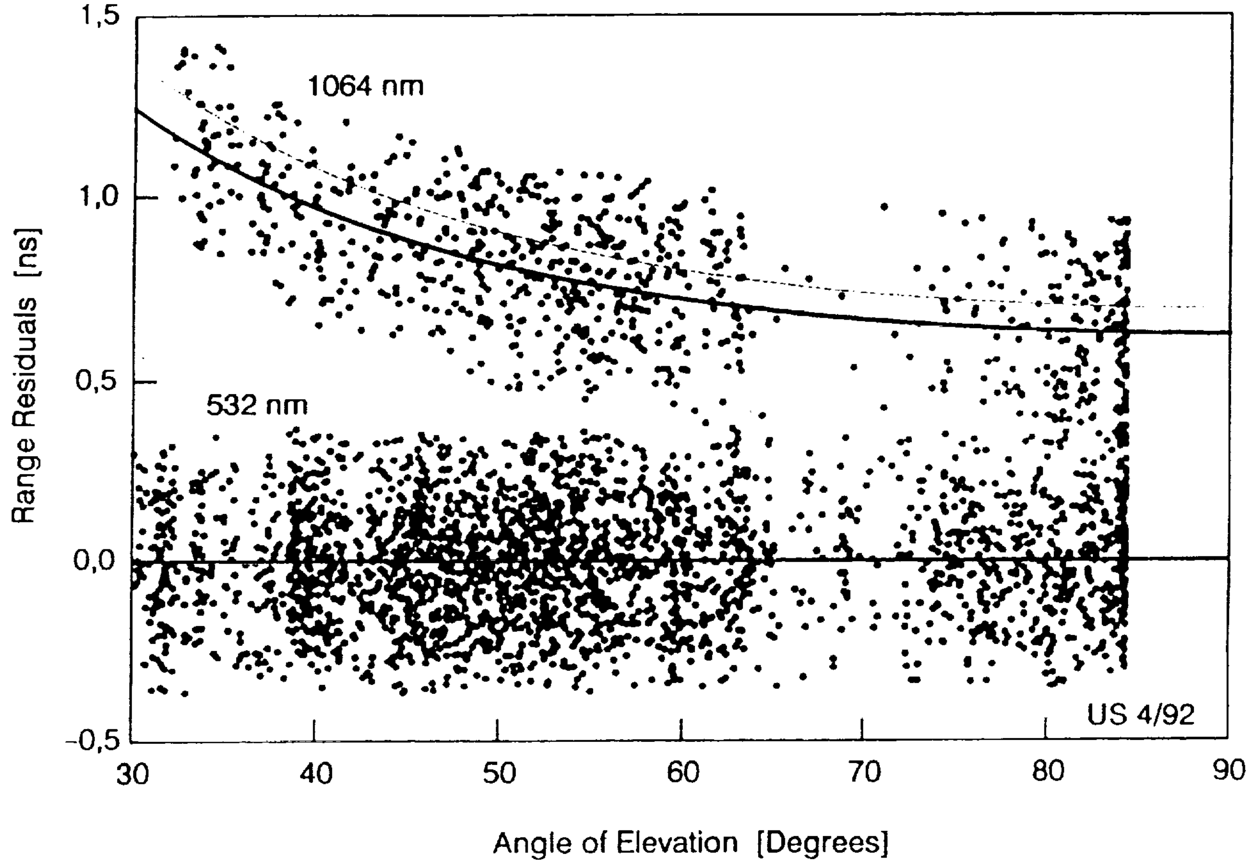

Figure 4: The range residuals of the two different frequency components plotted versus the angle of elevation (satellite: LAGEOS Oct. 4th 1991)

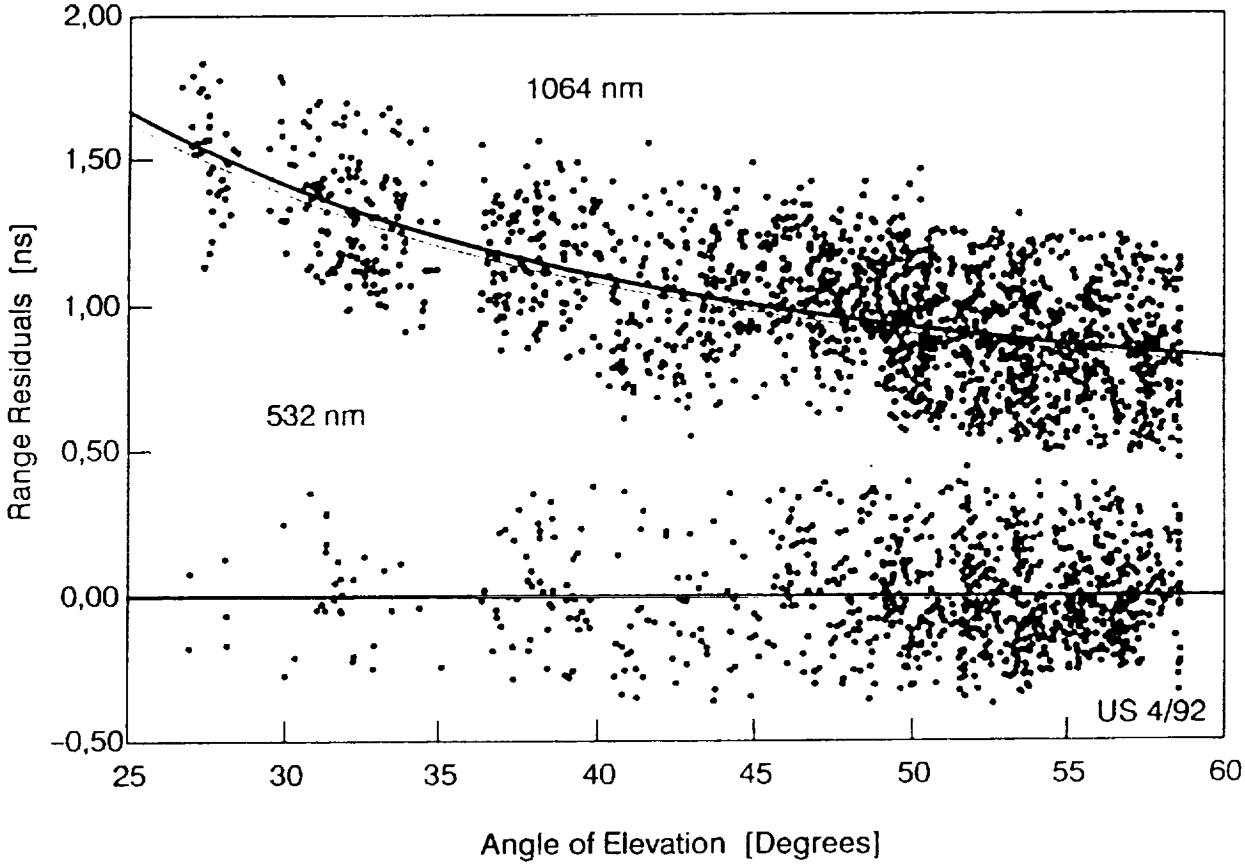

Figure 5: The range residuals of the two different frequency components plotted versus the angle of elevation (satellite: LAGEOS Mar. 8th 1992)

N94-15583

MILLIMETER ACCURACY SATELLITES FOR TWO COLOR RANGING

John J. Degnan
Code 901
NASA Goddard Space Flight Center
Greenbelt, MD 20771 USA

ABSTRACT

The principal technical challenge in designing a millimeter accuracy satellite to support two color observations at high altitudes is to provide high optical cross-section simultaneously with minimal pulse spreading. In order to address this issue, we provide, in this paper, a brief review of some fundamental properties of optical retroreflectors when used in spacecraft target arrays, develop a simple model for a spherical geodetic satellite, and use the model to determine some basic design criteria for a new generation of geodetic satellites capable of supporting millimeter accuracy two color laser ranging. We find that increasing the satellite diameter provides: (1) a larger surface area for additional cube mounting thereby leading to higher cross-sections; and (2) makes the satellite surface a better match for the incoming planar phasefront of the laser beam. Restricting the retroreflector field of view (e.g. by recessing it in its holder) limits the target response to the fraction of the satellite surface which best matches the optical phasefront thereby controlling the amount of pulse spreading. In surveying the arrays carried by existing satellites, we find that European STARLETTE and ERS-1 satellites appear to be the best candidates for supporting near term two color experiments in space.

1 INTRODUCTION

A companion article in these proceedings [Degnan, 1992] demonstrates the benefits of utilizing and maintaining ultrashort pulsewidths in performing two color ranging measurements to satellites. Unfortunately, even if one starts with a very short pulsewidth (e.g. 35 psec), most of the existing satellites will broaden the pulse significantly thereby degrading the precision of the differential time-of-flight measurement. This is especially true for the high altitude satellites, such as LAGEOS and ETALON, which are the primary targets for space geodesy applications. The principal technical challenge in designing a millimeter accuracy satellite to support two color observations at high altitudes is to provide high optical cross-section simultaneously with minimal pulse spreading. In order to address this issue, we provide, in this paper, a brief review of some fundamental properties of optical retroreflectors when used in spacecraft target arrays, develop a simple analytical model for spherical geodetic satellites, and use the model to determine some basic design criteria for a new generation of geodetic satellites capable of supporting millimeter accuracy two color laser ranging.

2 RETROREFLECTOR CHARACTERISTICS

For normally incident light, a single unspoiled retroreflector has a peak (on-axis) optical cross-section σ_{CC} defined by

$$\sigma_{cc} = \rho A_{cc}\left(\frac{4\pi A_{cc}}{\lambda^2}\right) \tag{2.1}$$

where ρ is the cube corner reflectivity, $A_{cc} = \pi R_{cc}^2$ is the light collecting area of the corner cube, and $4\pi A_{cc}/\lambda^2$ is the on-axis retroreflector gain. For a circular entrance aperture, the far field diffraction pattern (FFDP) of the reflected wave is the familiar Airy function given by [Born and Wolf, 1975]

$$\sigma(x) = \sigma_{cc}\left(\frac{2J_1(x)}{x}\right)^2 \tag{2.2a}$$

where

$$x = kR_{cc}\sin(\theta_1) \tag{2.2b}$$

The Airy pattern consists of a main central lobe surrounded by weak rings. The angular half-width from the beam center to the first null is given by the first nonzero root of the Bessel function J_1 which, with (2.2b), yields the formula

$$\theta_{null} = 1.22\frac{\lambda}{D_{cc}} \tag{2.3}$$

where λ is the wavelength and $D_{CC} = 2\ R_{CC}$ is the diameter of the retroreflector.

At arbitrary incidence angle, the area in (2.1) is reduced by the factor [Minott, 1974]

$$\eta(\theta_{inc}) = \frac{2}{\pi}(\sin^{-1}\mu - \sqrt{2}\mu\tan\theta_{ref})\cos\theta_{inc} \tag{2.4}$$

where θ_{inc} is the incident angle and θ_{ref} is the refracted angle determined by Snell's law, i.e.

$$\theta_{ref} = \sin^{-1}\left(\sin\frac{\theta_{inc}}{n}\right) \tag{2.5}$$

where n is the cube index of refraction. The quantity μ is given by the formula

$$\mu = \sqrt{1 - 2\tan^2\theta_{ref}} \tag{2.6}$$

Thus the peak optical cross-section in the center of the reflected lobe falls off as

$$\sigma_{eff}(\theta_{inc}) = \eta^2(\theta_{inc})\sigma_{cc} \tag{2.7}$$

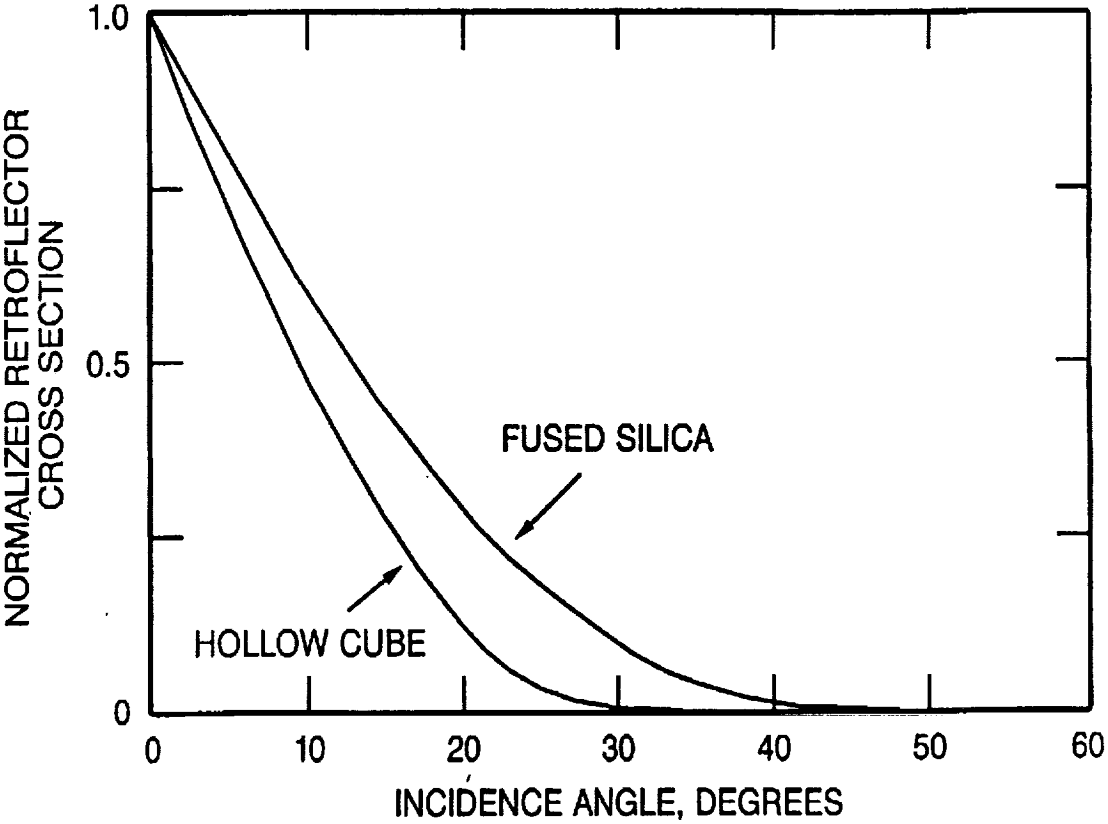

Figure 1: Normalized peak optical cross-section as a function of incidence angle for an unspoiled retroreflector.

Figure 1 shows the falloff of optical cross-section with incidence angle for the two most common retroreflectors - hollow ($n=1$) and quartz ($n=1.455$). Note that, for a solid quartz cube, the optical cross-section falls to half its on-axis value at roughly 13° incidence angle and is effectively zero beyond about 40°. The cross-section for a hollow cube corner falls to half its normal incidence value at about 9° and is effectively zero beyond about 30°.

One can further limit the effective incidence angle over which the retroreflector responds by recessing the reflector in its holder. It can be easily shown that the incidence angle at which the retroreflector response is zero is given by

$$\theta_{\max} = \cot^{-1}\left(\frac{d}{D_{cc}}\right) \tag{2.8}$$

where d is the depth of the recess.

3 VELOCITY ABERRATION

As mentioned previously, the far field diffraction pattern (FFDP) of a cube corner with a circular entrance pupil function corresponds to the familiar Airy pattern consisting of a single main lobe surrounded by low intensity rings. If there were no relative motion between the satellite and the target, the center of the FFDP would fall on the instantaneous line of sight between the target and satellite. However, due to the relative velocity between the satellite and the target, the coordinates of the FFDP are translated. The magnitude of the angular displacement in the FFDP is given by the equation [Minott, 1976]:

$$\alpha(h_s, \theta_{zen}, \omega) = \alpha_{\max}(h_s)\sqrt{\cos^2\omega + \Gamma^2(h_s, \theta_{zen})\sin^2\omega} \tag{3.1}$$

where the maximum value, $\alpha_{\max}$, is given by the expression

$$\alpha_{\max}(h_s) = \frac{2}{c}\sqrt{\frac{R_E^2 g}{R_E + h_s}} \tag{3.2}$$

and

$$\Gamma(h_s, \theta_{zen}) = \sqrt{1 - \left(\frac{R_E \sin\theta_{zen}}{R_E + h_s}\right)^2} \tag{3.3}$$

and R_E is the Earth radius, $g = 9.8$ m/sec^2 is the gravitational acceleration at the surface, h_s is the satellite height above sea level, c is the velocity of light, and the angle

$$\omega = \cos^{-1}[(\hat{r} \times \hat{\rho}) \cdot \hat{v}] \tag{3.4}$$

where $\hat{r}$, $\hat{\rho}$, and $\hat{\upsilon}$ are all unity length vectors corresponding to the satellite position vector (relative to the Earth center), the line-of-sight vector between station and satellite, and the satellite velocity vector respectively. Since $\Gamma(h_s, \theta_{zen})$ is always less than unity, equation (3.1) has an effective "minimum" value for a given θ_{zen}, when $\omega = \pi/2$. Thus,

$$\alpha_{\min}(h_s, \theta_{zen}) = \alpha_{\max}(h_s)\Gamma(h_s, \theta_{zen}) \tag{3.5}$$

The maximum and minimum angular displacements of the FFDP are plotted as a function of satellite height in Figure 2 assuming a maximum θ_{zen} of 70°. It should be noted from the figure that the angular displacement decreases with altitude and that the maximum and minimum values converge for high satellites. At ETALON altitudes (19,000 Km), for example, the angular displacement is roughly constant at about 26 μrad.

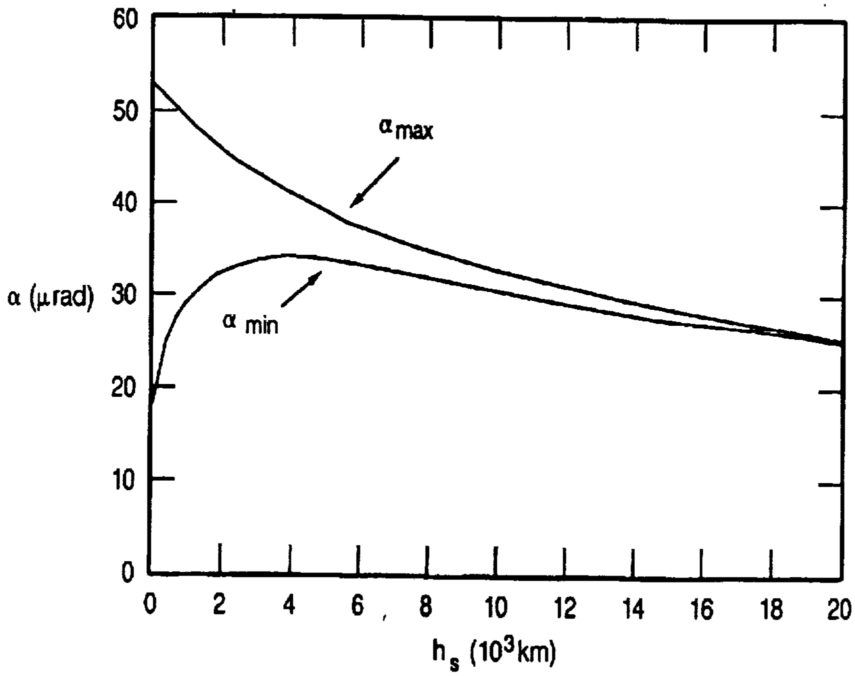

Figure 2: Maximum and minimum angular displacements in the retroreflector far field diffraction pattern caused by the velocity aberration effect as a function of satellite altitude above the Earth's surface.

If the target FFDP is angularly narrow relative to the size of the velocity aberration displacement, the receiver will lie on the low signal edge of the FFDP or even lie outside the FFDP entirely. For example, consider a moving retroreflector whose face is normal to the ranging system line-of-sight. The cross-section is given by (2.2a) with $x = kR_{cc}\sin(\alpha) \sim kR_{cc}\alpha$ where alpha is the instantaneous angular displacement caused by velocity aberration. If $\alpha \ll \alpha_{null}$, the reduction in cross-section is negligible. However, if α is large, the reflected beam will "miss" the receiver and low or nonexistent signal levels will result. For non-normal incidence angles, the reflected FFDP is no longer circularly symmetric since the collecting (and transmitting) aperture of the retroreflector appears as an ellipse to the range receiver. The FFDP peak is again along the instantaneous receiver line-of-sight, but the FFDP is now given by the two-dimensional Fourier transform of the elliptic entrance aperture of the corner cube. The velocity aberration causes the retroreflector response to be reduced relative to the peak value given by (2.7). This reduction is greater for velocity vectors which are parallel to the long axis of the ellipse because of the faster falloff of the FFDP with angle in this direction.

4 RETROREFLECTOR "SPOILING"

To reduce the effects of velocity aberration in large retroreflectors, the retroreflector is often "spoiled". The goal of "spoiling" is to concentrate more reflected energy into the annular region bordered by α_{max} and α_{min}. Ideally, one would like to uniformly spread the energy within the annular ring yielding an optimum cross-section given by

$$\sigma_{ideal} = \rho A_{cc}\left(\frac{4\pi}{\Omega_{cc}}\right) = \rho A_{cc}\left(\frac{4}{\alpha_{max}^2 - \alpha_{min}^2}\right) \tag{4.1}$$

where the quantity in parentheses is the effective target gain and Ω_{cc} is the solid angle subtended by the annular ring of interest. However, conventional spoiling techniques generally result in average optical cross-sections which agree only within an order of magnitude with the ideal limit described by (4.1).

Spoiling is usually accomplished by introducing slight variations into the cube corner dihedral angles (typically less than two arcseconds). This creates a complicated FFDP which, for an incident beam normal to the cube face, breaks the initial single main Airy lobe into 2N lobes (where N = 1 to 3 is the number of spoiled dihedral angles) distributed within an angular annulus. The mean angular radius of the annulus increases linearly with the dihedral offset angle from a perfect cube and, from diffraction theory [see (2.3)], one expects the effective width of the various lobes to depend inversely on cube diameter.

Each of the 2N lobes originates from a different sector of the retroreflector entrance aperture. In fact, the FFDP of each lobe is determined by the two-dimensional Fourier transform of the projection of the $180^{\circ}/2N$ sector of the (assumed) circular retroreflector entrance aperture into a plane perpendicular to the line-of-sight between the satellite and the station. The distribution of energy within this "annulus" is therefore highly nonuniform. Furthermore, the effective area for each lobe is reduced to:

$$A_{eff} = \eta(\theta_{inc}) \frac{A_{cc}}{2N} \tag{4.2}$$

Substituting the latter expression into (2.1), we obtain an approximate expression for the peak optical cross-section at the center of one of the 2N lobes for the spoiled retroreflector at arbitrary incidence angle

$$\sigma_{peak}(\theta_{inc}, N) = \eta^2(\theta_{inc}) \frac{\sigma_{cc}}{(2N)^2} \tag{4.3}$$

One can also "spoil" the retroreflector by placing or grinding a weak lens onto the entrance face. This approach retains the single central lobe of the unspoiled cube corner while reducing its peak amplitude and spreading the energy over a wider solid angle, Ω. This yields a peak cross-section given by

$$\sigma_{lens} = \rho A_{cc} \left(\frac{4\pi}{\Omega} \right) \tag{4.4}$$

and can be an effective approach when velocity aberrations are sufficiently small.

5 SATELLITE OPTICAL CROSS-SECTION

As noted previously, the optical cross-section which can be achieved with a single retroreflector is limited by the need to compensate for velocity abberation effects. Received SLR signals can only be enhanced by summing the contributions of several retroreflectors. Modern geodetic target satellites (e.g., STARLETTE, LAGEOS, and ETALON) are all designed to be spherical in shape in order to avoid the large pulse spreading caused by earlier flat panel arrays when viewed at non-normal incidence. The spherical shape also simplifies the modelling of nonconservative forces acting on the satellite.

Satellite array size is largely determined by the satellite altitude since more retroreflectors are required to achieve reasonable signal-to-noise ratios over longer slant ranges. Thus, STARLETTE (960 Km), LAGEOS (5900 Km), and ETALON (19,200 Km) have diameters of 12, 60, and 129.4 cm and average optical cross-sections of .65, 7, and 60 million square meters respectively.

Let us consider a spherical satellite which is uniformly covered with retroreflectors. The density of cube corners, as a function of incidence angle, is easily seen to be

$$N(\theta_{inc}) d\theta_{inc} = \frac{N}{2} \sin\theta_{inc} d\theta_{inc} \tag{5.1}$$

where N is the total number of reflectors on the satellite. To obtain a simple expression for the overall target cross-section σ, we approximate the sum over all of the retroreflectors within the allowed range of incidence angle by the following integral

$$\sigma = \sigma_{cc} \int_0^{\frac{\pi}{2}} d\theta_{inc} N(\theta_{inc}) \eta^2(\theta_{inc}) \tag{5.2}$$

where we have used (2.7). If the retroreflectors are not recessed in their holders, $\eta(\theta_{inc})$ is given by (2.4). If their angular response is limited by the recess, the variation can be well-approximated by the expression

$$\eta(\theta_{inc}) = 1 - \frac{\theta_{inc}}{\theta_{\max}} \tag{5.3}$$

where $\theta_{\max}$ is given by (2.8). Actually, (5.3) is an excellent approximation to (2.4) as well provided we choose $\theta_{\max}$ equal to .54 rad (31°) for hollow cubes or .75 rad (43°) for solid cubes respectively (see Figure 1). Substituting (5.2) and (5.3) into (5.2) and evaluating the resulting integrals yields

$$\sigma = \frac{\sigma_{cc} N}{2} \left[1 - \frac{\sin^2\left(\frac{\theta_{\max}}{2}\right)}{\left(\frac{\theta_{\max}}{2}\right)^2} \right] \tag{5.4}$$

Let us now examine the validity of (5.4) by substituting LAGEOS values. The LAGEOS satellite has a radius R = 29.8 cm and is imbedded with 426 retroreflectors (422 fused quartz and 4 germanium) with a clear aperture diameter D_{CC} of 3.81 cm. Ignoring the fact that four cubes are germanium, we choose N = 426 and a value of $\theta_{\max}$ = .75 rad for solid quartz cubes. We now use a value σ_{cc} = 2.834 x 10^6 in agreement with the input values to the RETRO computer program as determined during LAGEOS testing and evaluation [Fitzmaurice et al, 1977]. Substituting the latter values into (5.4) yields

$$\sigma_{LAGEOS} = 9.8\sigma_{cc} = 2.78 x 10^7 m^2 \tag{5.5}$$

This is roughly equal to the peak value computed by the much more detailed RETRO program which showed a range of values between .54 and 2.7 x 10^7 m^2. Equation (5.4) tends to overestimate the actual cross-section because it includes only geometric, and not velocity aberration, effects. Equation (5.5) also implies that the LAGEOS array cross-section is roughly 9.8 times that of a single cube corner at normal incidence.

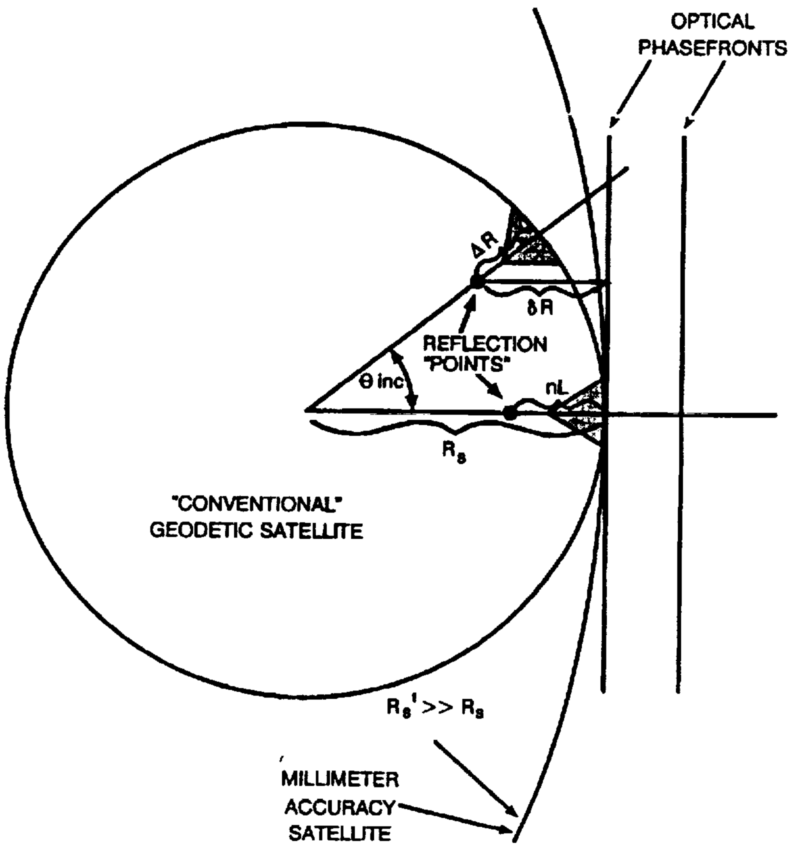

Figure 3: Diagram of a spherical geodetic satellite defining the variables used in the analysis.

6 SATELLITE IMPULSE RESPONSE AND TARGET SPECKLE

An individual retroreflector responds as a point source and hence does not spread the laser pulse in time. However, with a typical array of retroreflectors, the laser pulse arrives at the "reflection center" of each retroreflector at a slightly different time leading to a broadening of the received pulse [Degnan, 1985]. The location of the "reflection center" for an individual solid cube corner reflector is given by [Fitzmaurice et al, 1977; Arnold, 1978]

$$\Delta R(\theta_{inc}) = nL\sqrt{1-\left(\frac{\sin\theta_{inc}}{n}\right)^2} = nL\cos\theta_{ref} \tag{6.1}$$

where $\Delta R(\theta_{inc})$ is measured from the center of the front face of the cube corner to the reflection point, L is the vertex to front face dimension, n is the refractive index of the corner cube material, θ_{inc} is the angle of incidence, and θ_{ref} is the corresponding refraction angle. From Figure 3, it can be seen that a cube at an angle θ_{inc} to the incident wave produces a time delay, relative to the surface of the satellite closest to the ranging station ($\theta_{inc} = 0$), given by

$$\Delta t(\theta_{inc}) = \frac{2}{c}\{R_s - [R_s - \Delta R(\theta_{inc})]\cos\theta_{inc}\} = \frac{2R_s}{c}\left\{1 - \cos\theta_{inc}\left[1 - \frac{nL}{R_s}\cos\theta_{ref}\right]\right\} \qquad (6.2)$$

where R_s is the satellite radius. It should also be noted that the differential delay between target reflection points also introduces a random phase delay between individual reflectors. Thus, if the temporal profiles from multiple cubes overlap at the range receiver, the electric fields will interfere with each other in a random way from shot to shot resulting in target "speckle". On average, however, the return waveform from the satellite should behave as if each of the retroreflectors is an incoherent source. This was an implicit assumption in our derivation of target optical cross-section in Section 5.

In the same spirit, the time-averaged satellite impulse response can be estimated by summing the weighted (incoherent) returns from each of the retroreflectors. Using the simple model for a spherical satellite introduced in Section 5, the impulse response can be shown to be

$$I(t) = \sigma_{cc}\frac{N}{2}\int_0^{\frac{\pi}{2}} d\theta_{inc}\sin\theta_{inc}\eta^2(\theta_{inc})\delta[t - \Delta t(\theta_{inc})] \qquad (6.3)$$

where the geometric weighting factor is given by (2.4) or (5.3), $\Delta t(\theta_{inc})$ is given by (6.2), and the delta function $\delta[t - \Delta t(\theta_{inc})]$ represents an infinitely short laser pulse waveform incident on the satellite. From (6.2), we see that the delta function is nonzero only when the condition

$$\cos\theta(\tau,\epsilon,n) = \frac{1-\tau}{1 - \epsilon\sqrt{1 - \frac{1}{n^2} + \left[\frac{\cos\theta(\tau,\epsilon,n)}{n}\right]^2}} \qquad (6.4)$$

holds where we have defined the new variables

$$\tau = \frac{ct}{2R_s} \qquad \epsilon < \tau < \tau_{\max}$$

$$\epsilon = \frac{nL}{R_s} \qquad \tau_{\max} = 1 - \cos\theta_{\max}\left[1 - \epsilon\sqrt{1 - \frac{1}{n^2} + \left(\frac{\cos\theta_{\max}}{n}\right)^2}\right] \qquad (6.5)$$

The variable τ is a normalized time, expressed in units of the roundtrip transit time from the surface of the satellite to the center and back, and ϵ is the ratio of the optical depth of the cube to the satellite radius. The minimum and maximum values of τ

are determined by setting θ equal to zero and $\theta_{\max}$ respectively in (6.4) and solving for τ. The total pulse duration, measured at the baseline, is given by $\Delta t = t_{\max} - \epsilon$.

From (5.3) and (6.3), the satellite impulse response can now be expressed as a function of the variables τ, ϵ, n, and $\theta_{\max}$, i.e.

$$I(\tau,\epsilon,n,\theta_{\max}) = \sigma_{cc}\frac{N}{2}\sin\theta(\tau,\epsilon,n)\left[1-\frac{\theta(\tau,\epsilon,n)}{\theta_{\max}}\right]^2 \tag{6.6}$$

where $\theta(\tau,\epsilon,n)$ is defined by (6.4). In the limit of large satellite diameters ($\epsilon \to 0$), (6.4) reduces to the simple form

$$\theta(\tau,0,n) = \cos^{-1}(1-\tau) \tag{6.7}$$

and (6.6) becomes

$$I(\tau,0,n,\theta_{\max}) = \sigma_{cc}N\sqrt{\frac{\tau}{2}\left(1-\frac{\tau}{2}\right)}\left[1-\frac{\cos^{-1}(1-\tau)}{\theta_{\max}}\right]^2 \tag{6.8}$$

The quantity ϵ is typically small and, for nonzero values of ϵ, (6.4) can be easily solved by iteration using (6.7) as a starting point, i.e.

$$[\cos\theta(\tau,\epsilon,n)]_{j+1} = \frac{1-\tau}{1-\epsilon\sqrt{1-\frac{1}{n^2}+\left[\frac{[\cos\theta(\tau,\epsilon,n)]_j}{n}\right]^2}} \tag{6.9}$$

until it converges.

As an illustration, let us use (6.6) to estimate the impulse response of the LAGEOS satellite. Substituting n = 1.455 (fused silica), L= 1.905 cm, and R_S = 29.8 cm into (6.5b), we obtain a value $\epsilon = .093$. We recall that, for solid cube corners, we can use a value $\theta_{\max} = .75$ rad. Now, using (6.6) and (6.9), we obtain the plot of the LAGEOS impulse response shown in Figure 4(a). The profile shows the characteristic fast rise and long tail of the LAGEOS response. Furthermore, if we compute a center-of-mass correction from the centroid of this impulse response profile, we obtain a value of 250.2 mm which is in excellent agreement with the accepted LAGEOS value of 249 ± 1.7 mm [Fitzmaurice et al, 1977].

The impulse response in the large satellite limit, given by (6.8), is shown in figure 4(b) for the case of solid quartz and hollow cubes. Note that both the temporal width of the reflected pulse and the target optical crossection is smaller for the hollow cubes than for the solid cubes because of their smaller field of view.

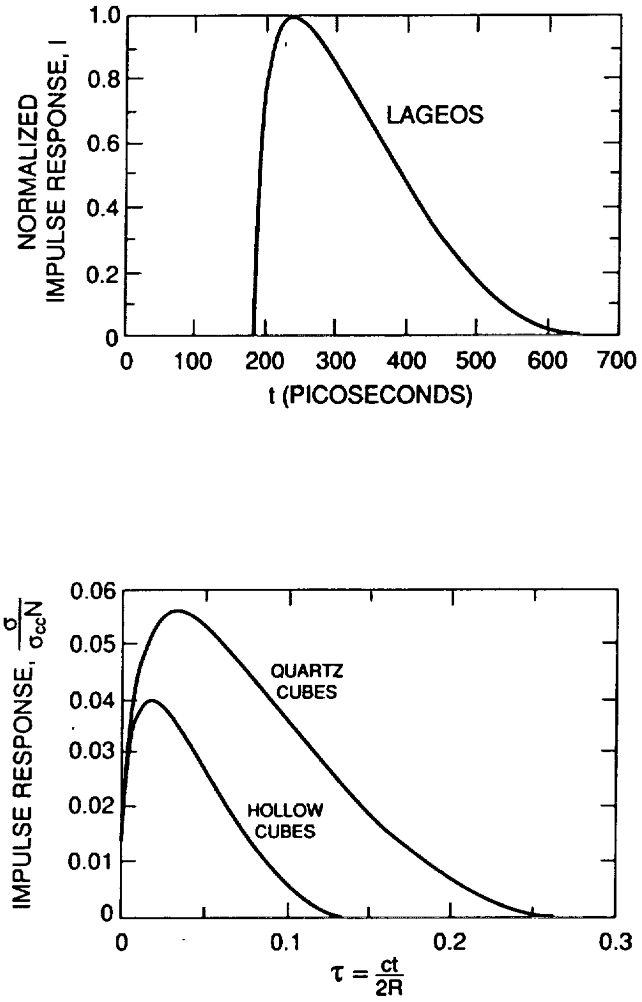

Figure 4: (a) Impulse response of the LAGEOS satellite as computed by our simple analytical model. (b) Impulse response in the large satellite limit for both hollow and solid quartz cubes.

7 FEASIBILITY OF MILLIMETER ACCURACY SATELLITES

We will now demonstrate that, in order to achieve high optical cross-section simultaneously with minimal pulse spreading with a spherical satellite, we must increase the satellite diameter and/or retroreflector density and simultaneously restrict the response to retroreflectors within a relatively small solid angle on the satellite surface about the station line of sight.

The total time duration of the reflected pulse (0% to 0% intensity points) can be determined from (6.5), i. e.

$$\Delta t=\frac{2R_s}{c}(\tau_{\max}-\epsilon)=\frac{2R_s}{c}\left\{2\sin^2\frac{\theta_{\max}}{2}+\epsilon\left[\cos\theta_{\max}\sqrt{1-\frac{\sin^2\theta_{\max}}{n^2}}-1\right]\right\} \tag{7.1}$$

which, in the limit of small maximum incidence angles, reduces to

$$\Delta t\sim\frac{R_s}{c}\theta^2_{\max}\left[1-\epsilon\left(1+\frac{1}{n^2}\right)\right] \tag{7.2}$$

In the same limit, Eq. (5.4) for the satellite optical cross-section reduces to

$$\sigma\sim\frac{\sigma_{cc}N}{24}\theta^2_{\max} \tag{7.3}$$

As mentioned earlier, the angular response can be restricted by recessing the retroreflectors in their holders. Substituting (7.2) into (7.3) yields

$$\sigma=\frac{\sigma_{cc}N}{24}\frac{c\Delta t_{\max}}{R_s\left[1-\frac{nL}{R_s}\left(1+\frac{1}{n^2}\right)\right]} \tag{7.4}$$

We can now express the total number of retroreflectors as

$$N=4\beta\frac{R^2_s}{R^2_{cc}} \tag{7.5}$$

where β is a "packing density" (= .435 for LAGEOS) which represents the fraction of total surface area occupied by the cube faces. Substituting (7.5) into (7.4) yields our final result

$$\sigma\sim\frac{\sigma_{cc}}{6R^2_{cc}}\frac{\beta R_s c\Delta t}{\left[1-\frac{nL}{R_s}\left(1+\frac{1}{n^2}\right)\right]} \tag{7.6}$$

The product $\beta R_s c\Delta t$ in (7.6) quantifies our earlier statement that, if we wish to reduce the amount of pulse-spreading Δt by some factor (via reduction of the retroreflector field-of-view), we must increase the retroreflector packing density -satellite radius product (βR_s) by the same factor to retain a similar target cross-section.

8 CONCLUSION

As mentioned previously, the principal technical challenge in designing a millimeter accuracy satellite to support two color observations at high altitudes is to provide high optical cross-section simultaneously with minimal pulse spreading. Increasing the satellite diameter provides: (1) a larger surface area for additional cube mounting thereby leading to higher cross-sections; and (2) makes the satellite surface a better match for the incoming planar phasefront of the laser beam as in Figure 3. Simultaneously restricting the retroreflector field of view (e.g. by recessing it in its holder) limits the target response to the fraction of the satellite surface which best matches the optical phasefront thereby reducing the amount of pulse spreading.

For near term experiments, the small radius of STARLETTE makes it an attractive target for testing and evaluating two color systems or for testing atmospheric models. Furthermore, its low altitude (960 Km) and moderate target cross section results in relatively high received signal levels. AJISAI, also in a relatively low 1375 Km orbit, consists of small clusters of retroreflectors separated by large reflecting panels and has comparable signal strength to STARLETTE. Unfortunately, the satellite is quite large and simultaneous returns from several retro clusters results in a complicated satellite signature [Prochazka et al, 1991]. From Figure 4, LAGEOS spreading is in excess of 150 picoseconds FWHM in agreement with [Fitzmaurice et al, 1977] although, with sufficiently short laser pulses (<50 psec), individual retro rings should be resolvable via streak cameras at certain satellite orientations. (Note that the simple satellite model presented here gives an average response over the full range of satellite orientations and shows none of the structure expected from a particular orientation). The LAGEOS pulse spreading combined with relatively low signal returns, measured at the few to several tens of photoelectron level for most systems, would make the necessary differential timing very difficult [Degnan, 1992].

Another useful target for two-color system evaluation is the recently launched European Earth Remote Sensing satellite, ERS-1. It flies at a relatively low altitude (<800 Km) and has a small compact target consisting of one nadir-viewing retroreflector surrounded by a uniformly spaced ring of eight identical cube corners at a nadir angle of 50°. Approximate modelling of this satellite by the author indicates that sharp returns consisting of one or two peaks (well separated) can be obtained from most viewing angles as illustrated in Figure 5. At nadir angles between 0° and 15°, the nadir viewing cube is dominant whereas, for nadir angles between 30° and 70°, the ring provides a sharp return at virtually all azimuthal angles. At nadir angles between about 15° and 30°, there is some overlapping of returns and pulse distortion.

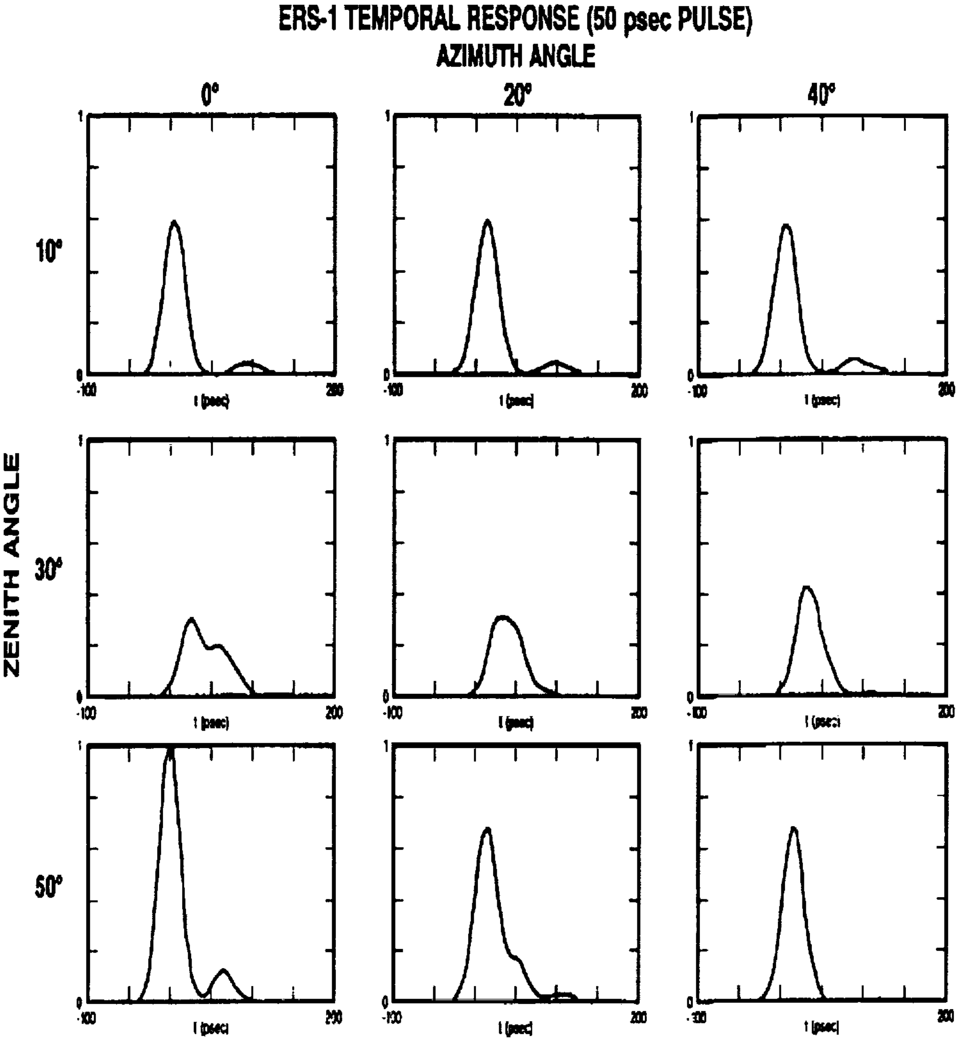

Figure 5: Approximate (geometric) response of the ERS-1 satellite to a 50 picosecond pulse as a function of nadir and azimuthal angle.

9 REFERENCES

Arnold, D. A., "Optical and infrared transfer function of the LAGEOS retroreflector array", Final Report NASA Grant NGR 09-015-002, Smithsonian Institution Astrophysical Observatory, May 1978.

Born M. and E. Wolf, "Principles of Optics", Chapter 8, Pergamon Press, New York, 1975.

Degnan, J. J., "Satellite laser ranging: current status and future prospects", IEEE Trans. on Geoscience and Remote Sensing, GE-23, pp. 398-413, 1985.

Degnan, J. J., "Optimum wavelengths for two color ranging", these proceedings, May 1992.

Fitzmaurice, M. W., P. O. Minott, J. B. Abshire, and H. E. Rowe, "Prelaunch testing of the Laser Geodynamic Satellite (LAGEOS)", NASA Technical Paper 1062, October 1977.

Minott, P. O., "Design of retrodirector arrays for laser ranging of satellites", NASA TM-X-723-74-122, Goddard Space Flight Center, March, 1974.

Minott, P. O., "Reader's Guide to the RETRO Program Output", NASA TM-X-722-76-267, Goddard Space Flight Center, September, 1976.

Prochazka, I., K. Hamal, G. Kirchner, M. Schelev, and V. Postovalov, "Circular streak camera application for satellite laser ranging", presented at SPIE Conference on Electronic Imaging, San Jose, California, Feb. 24-27, 1991.

TWO WAVELENGTH SATELLITE LASER RANGING USING SPAD

N94-15584

I.Prochazka, K.Hamal, H.Jelinkova

Faculty of Nuclear Science and Physical Engineering,Czech Technical University
Brehova 7, 115 19 Prague 1, Czechoslovakia
phone/fax +42 2 848840, tlx 121254, bitnet TJEAN@CSEARN.BITNET

G.Kirchner, F.Koidl

Lustbuehel Observatory,Lustbuehel str. 46,A-8042 Graz,Austria
phone +43 316 472231, fax +43 316 462678

GENERAL

When ranging to satellites with lasers, there are several principal contributions to the error budget : from the laser ranging system on the ground, from the satellite retro array geometry and from the atmosphere. Using a single wavelength we have been routinely achieved a ranging precision of 8 millimeters when ranging to the ERS-1 and Starlette satellites. The systematic error of the atmosphere, assuming the existing dispersion models, is expected to be of the order of 1 cm. Multiple wavelengths ranging might contribute to the refinement of the existing models. Taking into account the energy balance, the existing picosecond lasers and the existing receiver and detection technology, several pairs or multiple wavelengths may be considered. To be able to improve the atmospheric models to the subcentimeter accuracy level, the Differential Time Interval (DTI) has to be determined within a few picoseconds depending on the selected wavelength pair [1].

There exist several projects, based on picosecond lasers as transmitters and on two types of detection techniques : one is based on a photo detectors like photomultipliers or photodiodes connected to the time interval meters [5]. Another technique is based on the use of a streak camera as a echo signal detector,temporal analyzer and time interval vernier. The temporal analysis at a single wavelength using the streak camera showed the complexity of the problem [2].

EXPERIMENT SETUP

We are reporting on the novel concept of ranging to satellites at two wavelengths using a single solid state photon counter. The block scheme is plotted on Figure 1. The receiver package is based on the Silicon avalanche photodiode [4] capable of single photon detection. The receiver and detector is common for both wavelengths, the different color returns are separated in time due to the atmospheric dispersion. In principle, the use of common detector for both wavelengths results in system simplicity, stability and accuracy, as well. Most of the DTI measurement error contributions cancel out by averaging. The system calibration is simple and straightforward.

The experiment has been accomplished at the Satellite Laser Ranging Station Graz, Austria, employing the 0.5 meter aperture Contraves tracking telescope. Considering the available laser technology, the satellite laser telescope transmitter and receiver optics, namely the Coude path dielectric coatings, and the detector sensitivity, we have chosen the wavelength pair of 0.532 μm and 0.683μm proposed by J.Gaignebet [3]. The laser transmitter consists of the passively mode locked Quantel Nd:AG laser including the second harmonic generator, modified by inserting a Raman cell filled by Hydrogen at 25 Bars, delivering 15 mJ/35 psec at 0.532 μm and 5 mJ/25 psec at the 0.683 μm Stokes waves. Additionally, the anti Stokes radiation at 0.45 μm having the energy of 1-3 mJ is generated.

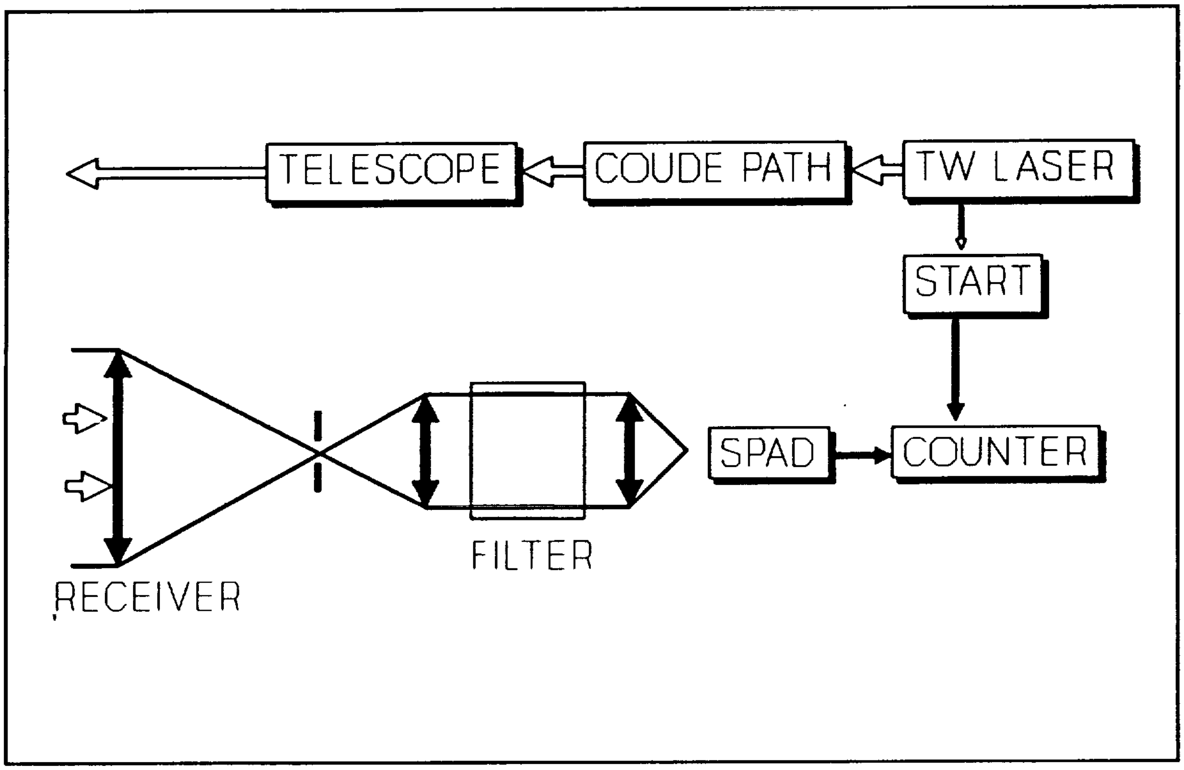

Figure 1 Two wavelengths laser ranging system setup using SPAD

RESULTS

Ranging to several ground targets we obtained a ranging precision of 42 picoseconds at 0.532 μm and 56 picoseconds at 0.683μm. The detector quantum efficiency at both these wavelengths reaches 20 %. The 6 kilometer distant ground target ranging results is shown on Figure 2. The first peak corresponds to 0.683 μm echoes, the second one to the 0.532 μm echoes. The measured DTI was 303.3 picoseconds. Taking into account the data of the atmosphere at this time, the calculated value is 299.4 picoseconds. The precision estimate of our DTI measurement is 4 picoseconds, if 400 returns per color are accumulated.

The first results of two wavelength laser ranging to the Ajisai satellite is on Figure 3, where the range residuals to the fitted orbit are plotted.The lower trace corresponds to the 0.683μm echoes, the upper one to the 0.532μm echoes. The DTI value variation along the pass is caused by changes in the satellite elevation and hence the atmospheric path difference. Up to now the satellites Lageos, ERS-1 and Ajisai have been ranged with two wavelengths. Typically a few hundreds of returns per pass and per wavelength have been collected when the system has been operating at 2.5 Hz. Averaging the two wavelengths data over the whole pass, the two wavelengths differential time interval has been determined with the precision typically 7 picoseconds.

2-COLOR RANGING TO TARGET

RESIDUALS of 532/683 nm Pulses

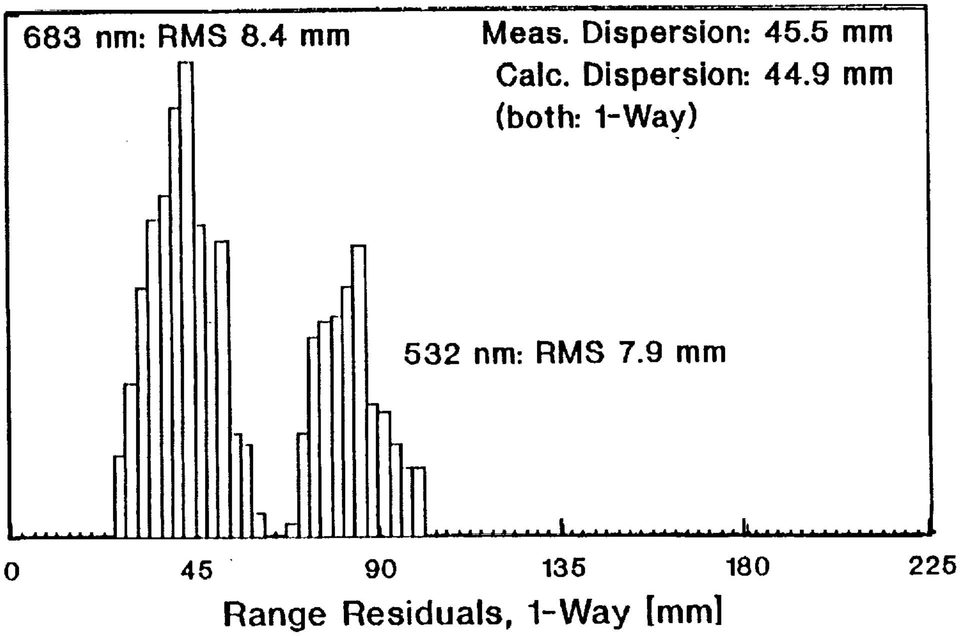

1991-12-12

Fig. 2

Satellite AJISAI

2-Color Ranging: 532 and 683 nm

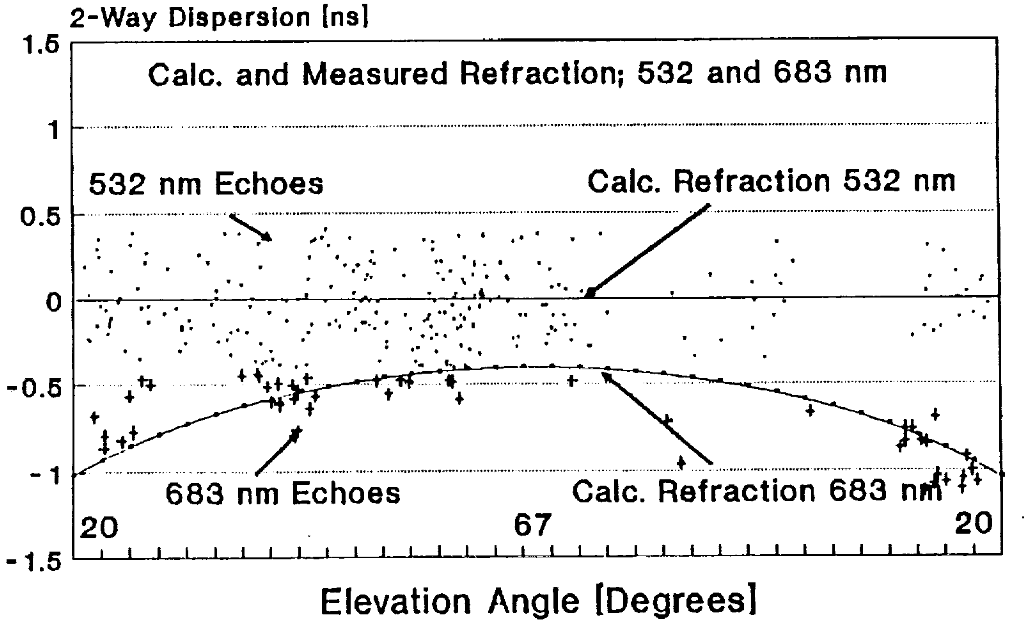

1991-12-12

Fig. 3

The energy budget, the number of returns per wavelength and hence the differential time interval precision has been limited by the system ranging repetition rate of 2.5 Hz, which is determined by the station ranging electronics. Additional limitation is the chromatic aberration of the transmitter refracting telescope, which limits the minimal divergence achievable simultaneously on both wavelengths. These two limitations are expected to be resolved within 1992.

CONCLUSION

Taking into account the energy budget when ranging to a satellite, assuming the data rate requested for two minute burst averaging and the ground target ranging results, one may conclude, that the picosecond accuracy of the two wavelength time difference interval is achievable using this technique. Comparing to the other two wavelengths ranging techniques, the simplicity, stability and the simple calibration is obvious. Some other wavelengths pairs, namely the Raman Stokes and anti Stokes, resulting in a considerably higher value of DTI may be considered. However, the telescope transmitter beam delivering optics has to be reconstructed.

References

1. J.B. Abshire, Applied Optics, Vol.19,No.20,1980, p34-36
2. I.Prochazka,K.Hamal,G.Kirchner,M.Schelev,V.Lozovoi,V.Postovalov, SPIE 1449-40
3. J.Gaignebet et al, Technical Digest of the Conference on Lasers and Electro Optics, CLEO 89, Baltimore, MD, 1989
4. I.Prochazka et al, technical Digest of the Conference on Lasers and Electro Optics, CLEO 90, Anaheim, CA, May 1990
5. B.Greene,proc.of the 6th International Workshop on Laser Ranging Instrumentation, Antibes,France, 1986

C-5

N94-15585

NEW PERSPECTIVES FOR HIGH ACCURACY SLR WITH SECOND GENERATION GEODESIC SATELLITES

Glenn LUND
Optical Department
AEROSPATIALE - Space & Defense Division
100 Boulevard du Midi
06322 CANNES LA BOCCA
FRANCE

ABSTRACT

This paper reports on the accuracy limitations imposed by geodesic satellite signatures, and on the potential for achieving millimetric performances by means of alternative satellite concepts and an optimised 2-colour system tradeoff.

Long distance laser ranging, when performed between a ground (emitter/receiver) station and a distant geodesic satellite, is now reputed to enable short arc trajectory determinations to be achieved with an accuracy of 1 to 2 centimeters. This state-of-the-art accuracy is limited principally by the uncertainties inherent to single-colour atmospheric pathlength correction. Motivated by the study of phenomena such as post-glacial rebound, and the detailed analysis of small-scale volcanic and strain deformations, the drive towards millimetric accuracies will inevitably be felt.

With the advent of short pulse (< 50 ps) *dual* wavelength ranging, combined with adequate detection equipment (such as a fast-scanning streak camera or ultra-fast solid-state detectors) the atmospheric uncertainty could potentially be reduced to the level of a few millimeters, thus exposing other less significant error contributions, of which by far the most significant will then be the morphology of the retroreflector satellites themselves.

Existing geodesic satellites are simply dense spheres, several 10's of cm in diameter, encrusted with a large number (426 in the case of LAGEOS) of small cube-corner reflectors. A single incident pulse thus results in a significant number of randomly phased, *quasi*-simultaneous return pulses. These combine coherently at the receiver to produce a convolved interference waveform which cannot, on a shot to shot basis, be accurately and unambiguously correlated to the satellite center of mass.

The present paper proposes alternative geodesic satellite concepts, based on the use of a very small number of cube-corner retroreflectors, in which the above difficulties are eliminated whilst ensuring, for a given emitted pulse, the return of a single clean pulse with an adequate cross-section.

1 RECENT AND IMMINENT ADVANCES IN SLR ACCURACY

Many SLR groups have reported, during the course of the present workshop, considerable progress in their laser station equipment, as well as in the performance of data reduction and orbital modeling.

Laser technology has made considerable progress since the days of the first ruby lasers, and most stations are now equipped with a doubled Nd:YAG. Pulse widths down to 50 ps, with an output power of ~ 30 mJ and a repeat rate of ~ 10 Hz are now being reported and can be expected to become routine performances in many stations. The temporal width of such pulses is now responsible for much less of the return signal duration than the optical depth of the satellite itself.

The technology of ultra-fast SPAD (Silicon Photo Avalanche Diode) detectors would seem very promising for picosecond event timing. Streak cameras, despite the considerable expense involved in their exploitation, are recognised not only for their single picosecond capacity but also for their ability to record single or multiple waveforms (eg. for 2-colour differential flight time measurements). K. Hamal has reported streak camera satellite signature recordings from AJISAI and STARLETTE.

The accuracy of atmospheric models, used to correct for the delay in pulse flight time, is considered to be limited by the small amount of meteorological data exploited and from which the entire atmospheric profile is implicitly defined. Although single-colour SLR makes use of a single *in situ* measurement of temperature pressure and water vapour pressure, 2-colour ranging is expected to enable a considerable improvement to be achieved by virtue of differential flight time correction. The residual error with this technique lies in the range of 2 to 3 mm.

Although several authors have reported improvements in the modeling used to take into account both gravitational and non-gravitational (radiation, thermal, drag) orbital influences, the residual bias in the determination of LAGEOS' orbit is estimated as 2 to 3 cm for 1 month of data and 1 cm for a year of data (R. Eanes). Many sophiticated data reduction and collation procedures have been elaborated, but the limit in rms baseline accuracy nevertheless appears to saturate at the level of 1 cm.

2 RETURN SIGNAL CONVOLUTION BY MULTIPLE ECHOS

The time domain behaviour of a round-trip SLR pulse can be thought of as an initially narrow Gaussian pulse which is convolved successively by the atmospheric transfer function (due to refractive index dispersion - typically ~ 10 ps), the "forest" of Diracs corresponding to each of the satellite reflectors "visible" at the ranging instant, the atmospheric transfer function for a second time, and finally the detector transfer function. Whereas the emission, detection and atmospheric functions could well provide a global received pulse FWHM of ~ 50 ps (7.5 mm), the satellite signature, determined by the overlapping reflector echos within its apparent optical depth, is typically an order of magnitude greater in duration.

The practically indeterminant and undeconvoluable nature of the resulting signature imposes a practical limit in residual range uncertainty varying between 1 and 5 cm (depending on the size and characteristics of the ranged satellite), even after several months of data accumulation. This uncertainty is represented by σ^2_{sat} (~ ≥ 100 ps) in expression (1) of §3.

In an effort to eliminate the drawbacks of such complex signatures, a novel geodesic satellite concept is proposed in which a very small number of retroreflectors, exhibiting very little or no local FOV overlap, is arranged in such a way as to ensure the unicity (or at least unambiguous identifiability) of the detected return waveforms. Ideally, the apexes of each retroreflecting cube corner would be mutually co-located at the satellite's centre of mass. In practice, this requirement cannot be exactly met, implying either some form of attitude stabilisation and/or deterministic correction between measured and true (centre of mass) ranges. The residual uncertainty in range correction should be no more than 1 or 2 mm.

Velocity aberration is a parameter of considerable importance, and the means used to achieve appropriate correction would depend on the implementation (or not) of attitude stabilisation.

Finally, an adequate systems approach to high accuracy SLR would require a careful tradeoff to be made between the mean satellite reflector cross-section (i.e. related to the cube corner size, mean incidence angle and diffraction lobe pattern) and station parameters such as (dual colour) laser wavelength choice, pulse energy and width, and receiving telescope size. The latter considerations are adressed on the following section.

3 LINK BUDGET REQUIREMENTS AND SYSTEM CONSIDERATIONS

The parameters which exert an influence on range accuracy include not only the retroreflector characteristics, but also the laser station design. Range accuracy and link budget analyses are thus needed in order to ascertain an optimal approach to the specification of high accuracy SLR satellites and 2-colour ranging stations, as set out below. The uncertainty in the absolute value of a 2-colour corrected normal point can be expressed as;

$$\sigma^2_{norm.pt.} = K_1 \left\{ \sigma^2_{sat} + \frac{\sigma^2_{noise}}{N_{shot}} + A^2 \left(\sigma^2_{sc} + \frac{1}{N_{shot}} \left(\frac{\sigma^2_{pulse}}{N_{det(\lambda 1)}} + \frac{\sigma^2_{pulse}}{N_{det(\lambda 2)}} \right) \right) \right\} \qquad (1)$$

where ;

- σ^2_{sat} is the unaccountable satellite center-of-mass bias,
- σ^2_{noise} is the cumulated random variance of the timing system,
- N_{shot} is the number of shots used to establish a normal point,
- K_1 is a conversion factor from ps to mm,
- σ^2_{sc} is the unaccountable Streak Camera bias (typically 1 to 2 ps),
- σ^2_{pulse} defines the received pulse width (σ = 0.425 FWHM),
- A is the 2-colour correction sensitivity (related to λ_1 and λ_2), and
- $N_{det(\lambda)}$ is the number of detected photons at wavelength λ.

The expected number of detected photons at a given wavelength is derived from the link budget analysis as follows :

$$N_{det} = K_2 \left\{ \lambda . \frac{1}{R^4(z)} . \frac{1}{\omega^2} . (1 - \theta/_{40}) . T^2_{atm}(z) . QE(\lambda) \right\} \times \left\{ \frac{E_{emit} . \Phi^2_{tel} . \Phi^2_{cc}}{\Omega^2} \right\} \qquad (2)$$

where ;

- K_2 is a constant including geometrical factors optical efficiencies,
- R is the station to satellite range,
- ω is the emitted beam divergeance,
- θ is the local incidence angle of the ranging beam relative to the reflector normal. *(1- θ/40)* gives a close approximation to the cube-corner cross-section falloff as a function of incidence angle),
- T_{atm} is the 1-way atmospheric transmission, depending on range angle **Z**,
- QE_λ is the receiver detector quantum efficiency at wavelength λ,
- E_{emit} is the emitted pulse energy,
- Φ_{tel} is the station receiving telescope diameter,
- Φ_{cc} is the retroreflector diameter, and
- Ω is the equivalent angular diameter of the retroreflector diffraction pattern.

Expression (2) has been grouped into two parts of which the first includes non-system or typically invariant parameters, whereas the second contains those variables which depend on the station (laser, telescope) and satellite (retroreflector size, diffraction pattern) designs.

The term σ_{pulse} in (1) is also considered as a system parameter, and has been combined with the second group of variables in (2) to form the quantity X_{syst} :

$$X_{syst:\,\sigma,E,\Phi_{tel},\Phi_{cc},\Omega} = \frac{E_{emit}.\Phi_{tel}^2.\Phi_{cc}^2}{\Omega^2.\sigma_{pulse}^2} \qquad \left(J.m^4.rad^{-2}.s^{-2}\right) \qquad (3)$$

Tradeoff analysis of the satellite and laser station characteristics can be made on the basis of the numerical evaluation of this quantity. Although the factor **A** is also a system-related parameter, its numerical value happens to be very similar for the 2 cases treated below and is there-fore not included in the above expression. In the following, it is assumed that Ω is <u>not</u> dependant on $Ø_{CC}$, but rather on an engineered diffraction lobe pattern; a conservatively large value of Ω is taken, corresponding to diffraction into a uniform ring 2.5 arcsecs in width, at a mean distance of 9 arcsecs from the incoming beam direction.

Figures (1) and (2) thus illustrate the computed variation of the 10-shot ranging accuracy $\sigma_{Norm.Pt.}$ (exp. 1) as a function of X_{syst}., for a 800 km circular orbit and negligeable center-of-mass bias (σ_{sat}), at four values of zenith ranging angle : 0°, 20°, 40° & 60° (assuming 10 km Standard Atmosphere visibility), and for two different cases of dual wavelength laser configuration :

Fig.1 Doubled & tripled Nd:YAG,
Fig.2 Fundamental & doubled (eg. Ti-Sapphire) wavelengths @ 800 & 400 nm.

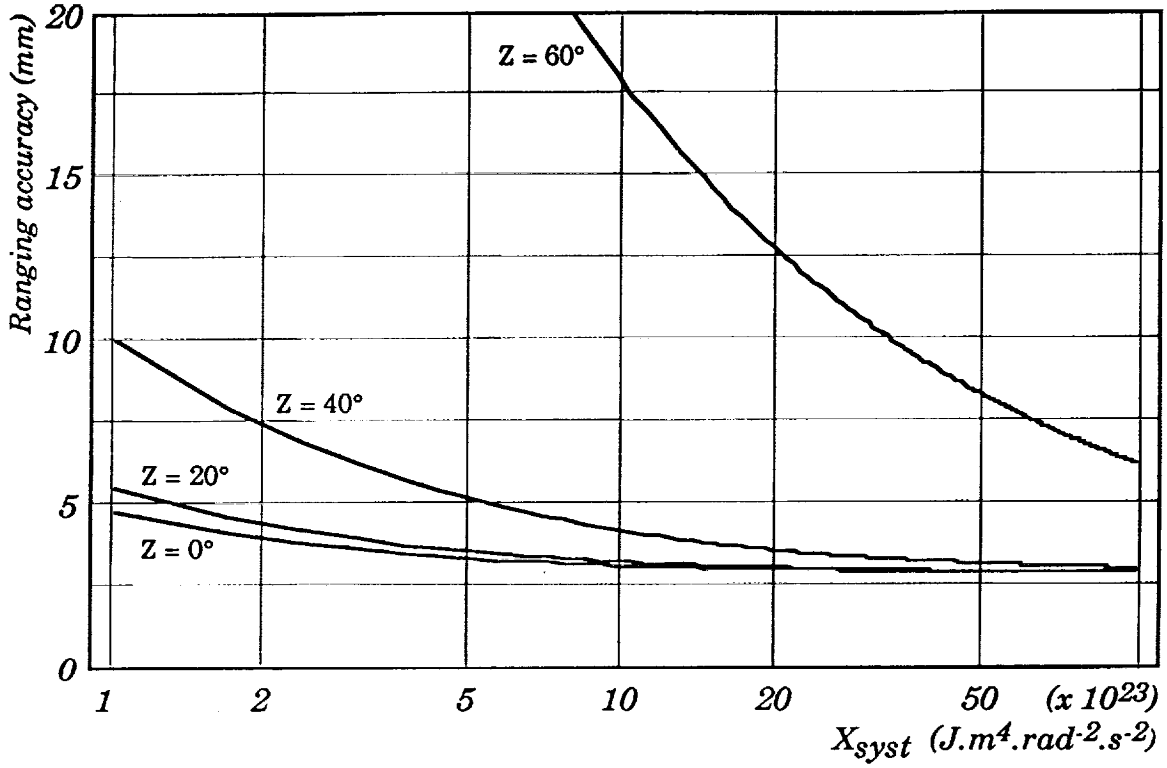

Figure 1. Nd:YAG 2-colour ranging accuracy as a function of the system input parameter X (= $E.\Phi^2_{tel}.\Phi^2_{cc} / \Omega^2.\sigma^2_{pulse}$) and zenith ranging angle Z.

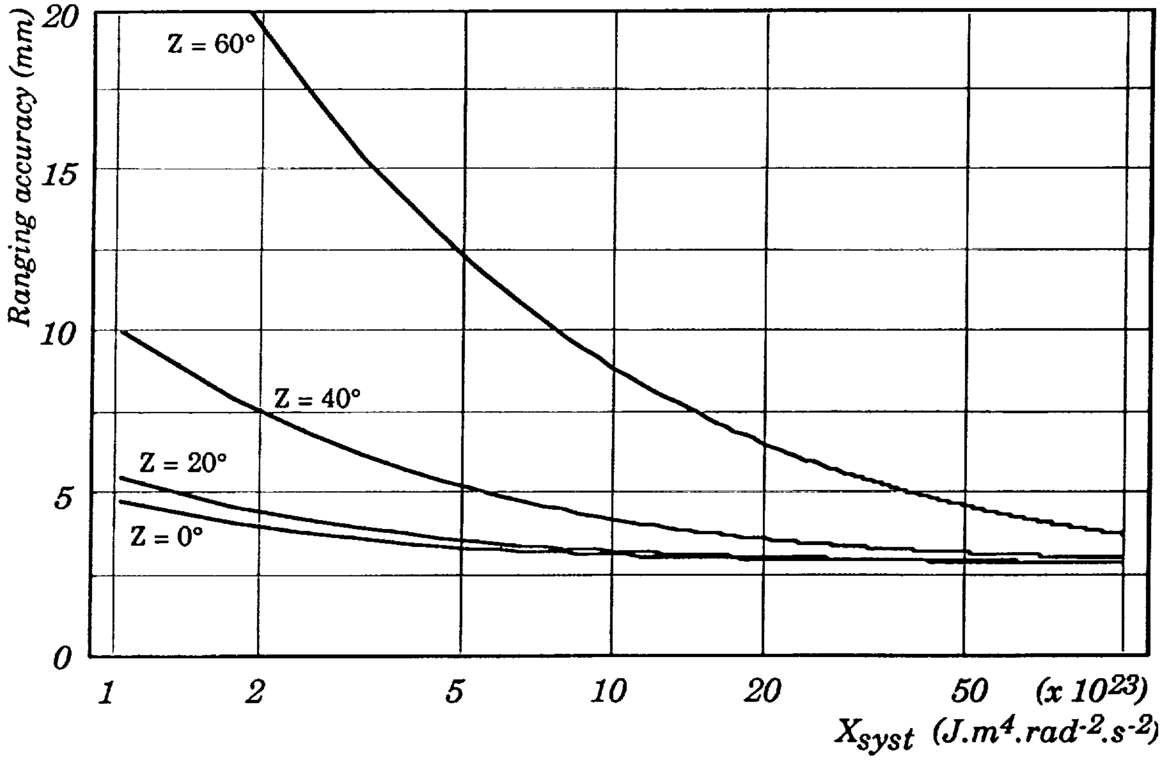

Figure 2. 400 / 800 nm 2-colour ranging accuracy as a function of the system input parameter X (= $E.\Phi^2_{tel}.\Phi^2_{cc} / \Omega^2.\sigma^2_{pulse}$) and zenith ranging angle Z.

The resulting curves show (for example) that if sub-centimetric ranging accuracies are to be achieved with 2-colour systems up to zenith angles of 60°, one could accept a value of $X_{syst.} \geq 7.10^{23}$ from the fundamental/doubled system, whereas a factor of ~ 8 improvement would be needed for comparable performance from a Nd:YAG station.

The above example supposes *normal* incidence at the retroreflector, and could be provided by the following numerical values for a 800 / 400 nm system and a *single* cube-corner retroreflector :

- E_{emit} = 40 mJ
- Φ_{tel} = 30 cm
- Φ_{cc} = 4 cm
- σ_{pulse} = 43 ps ($FWHM_{pulse}$ = 100 ps)

By shortening the emitted pulse FWHM to ~ 50 ps, one could achieve the same performance at local retroreflector incidences up to *30°*. An additional factor of ~ 3 improvement in telescope or reflector diameter would be required to achieve the same result with a Nd:YAG laser (assuming 40 mJ and 50 ps FWHM to be near to the practical limits for the emitted pulse power).

Further improvements could be achieved with still shorter pulses (in the case of a broad bandwidth amplification medium), or a larger number of pulses per normal-point. At the satellite level, larger retroreflectors, or more confined diffraction lobe patterns could be considered, without having to resort to the classical multiple reflector solution.

The strong link budget dependance on orbital height ($\propto R^{-4}$) would probably render single-reflector satellites unsatisfactory for orbits higher than a few 1000 km, if sub-centimetric accuracies were to be expected at high zenith angles and with a small number of pulses per normal point.

These considerations are encouraging, as they suggest that millimetric center-of-mass determinations could well be achieved with dual-colour SLR, provided appropriate consideration is given to the design of future geodesic satellites.

4 SECOND GENERATION REFLECTOR SATELLITE CONFIGURATIONS

It has been pointed out at the beginning of this paper that in the interests of a clean return signature and unambiguous center-of-mass determinations, the "ideal" geodesic satellite should exhibit non-overlapping reflector FOVs in order to inhibit multiple echo returns, whereas the link budget calculations given in § 3 show that a *single* retroreflector of reasonable dimensions could provide adequate return signal strength for millimetric range determination accuracies.

A parameter of considerable importance in the retroreflector design is that of velocity aberration correction, in which an appropriate trade-off is needed between link budget considerations (influenced by the value of Ω) and stabilisation of the reflector orientation relative to the orbital plane. Two fundamentally different approaches could thus be used, according to the choice between ultimate satellite simplicity and optimal link budget performance, as set out in the examples below :

4.1 UNSTABILISED OMNIDIRECTIONAL RETROREFLECTOR SATELLITE

An *omnidirectional* diffraction pattern, as used in the example in § 3 and in the case of existing geodesic satellites, relieves the spacecraft from any attitude stabilisation requirements, and thus results in the simplist form of satellite configuration. In the example shown in figure (3), the satellite is composed of 8 cube corner retroreflectors (solid or hollow, depending on thermal, optical and dimensional constraints), each designed to provide an annular diffraction lobe.

If the ranging system and satellite were designed so as to meet the link budget requirements for local incidence angles up to 30°, it can be shown that any emitted pulse would have a 55% probability of returning to the reciver with adequate signal strength. When compared with the potential advantage of highly accurate range determinations, the drawback of intermittently weak return signals does not appear to be of significant concern.

Although the finite thickness of the cube corner walls would lead to a small residual uncertainty in the center-of-mass determination, this effect is found to be negligeable for wall thicknesses up to ~ 2 cm.

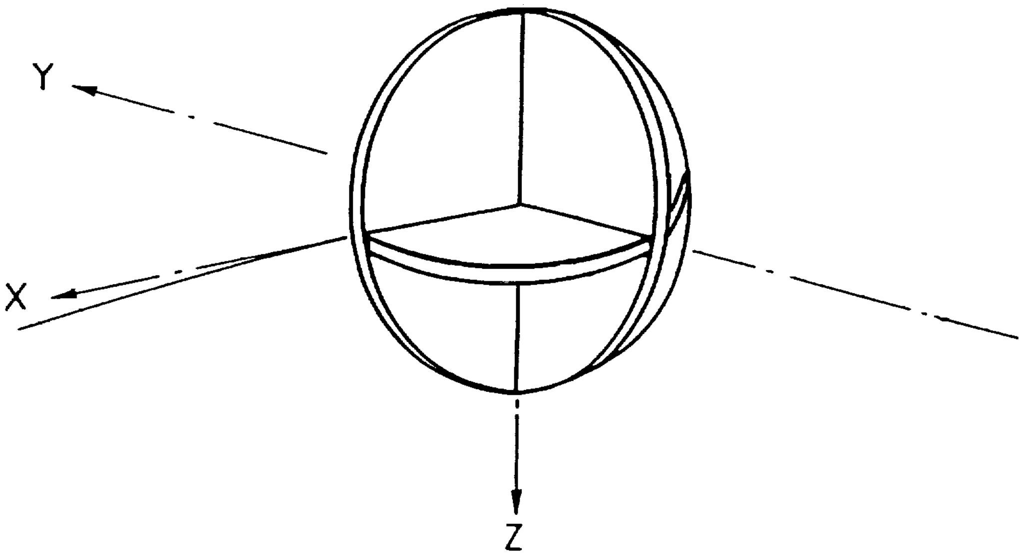

Figure 3 Passive geodesic satellite design for millimetric range determinations.

4.2 STABILISED DIRECTIONAL RETROREFLECTOR SATELLITE

The link budget performance of the previous design could be considerably improved by concentrating the diffracted energy into 2 small lobes (i.e. by reducing Ω), as is the case with the proposed GLRS-R ground target design (reported elsewhere in these proceedings). This approach could only be implemented if the direction of the diffraction lobes were appropriately maintained in alignment with the direction of relative movement between emitter and reflector.

In Figure (4), such a satellite design is shown, in which spin stabilised attitude control is used to maintain one of each of the cube corner dihedral angles in a direction perpindicular to the orbital plane. These dihedral angles would be slightly spoiled from perpindicularity so as to generate two small diffraction lobes in opposite directions, of sufficient amplitude to correct for the velocity aberration. A gain of - 10 or more in return signal strength, compared with the annular diffraction lobe design, could be expected.

Although a *spin* stabilisation is shown here, *3-axis* stabilisation could also be envisaged - thus requiring a smaller number of cube corners. In both cases the attitude control would not have to be very precise (typically - ± 5° should be adequate), and could be achieved using virtually passive systems such as magnetic torquers. A further possibility would be to use a completely passive 3-axis stabilisation system based on gravity masts.

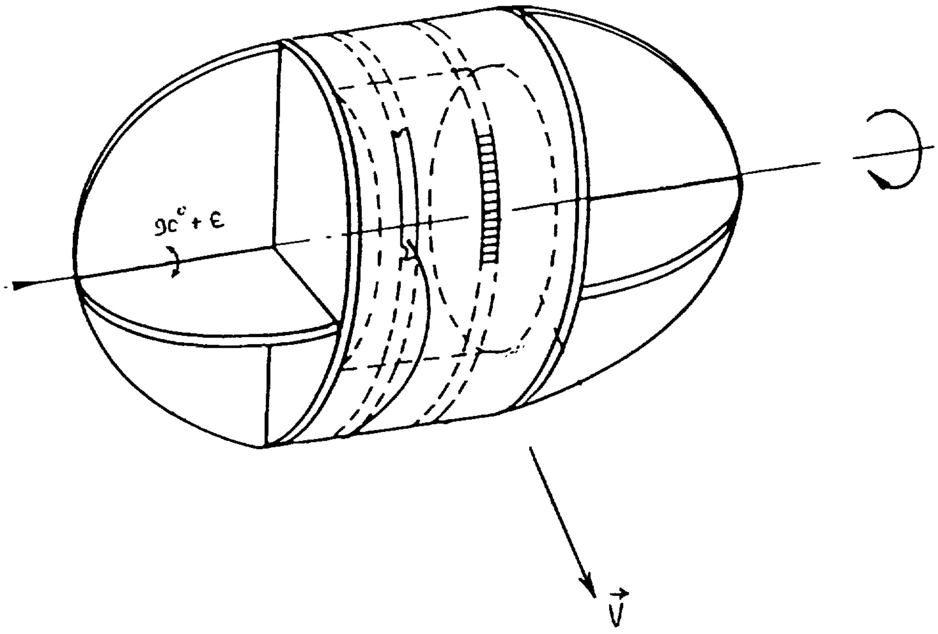

Figure 4 Spin-stabilised geodesic satellite design for millimetric range determinations.

5 CONCLUSIONS

It has been shown from link budget analyses that, when coupled with an appropriate satellite configuration, realistic *single* retroreflector dimensions could enable millimetric absolute accuracies to be achieved with future 2-colour SLR, through the removal of center-of-mass uncertainties in the range determination.

The engineering of retroreflector velocity aberration corrections is an important factor in the design of a geodesic satellite and in the link budget performance to be expected from the complete ranging system.

Two approaches to the design of second generation geodesic satellites have been suggested. Although these might imply the use of non-spherical orbiting bodies, with consequently higher atmospheric drag and solar radiation pressure imbalances than for existing satellites, they could nevertheless enable excellent geometric mode (short arc) range determinations to be achieved, and could be expected to provide very good long arc performance for high altitude orbits.